DEVELOPMENT OF MAGNESIUM BASED NEGATIVE ELECTRODE MATERIALS FOR NICKEL METAL HYDRIDE BATTERIES

A THESIS SUBMITTED TO
THE GRADUATE SCHOOL OF NATURAL AND APPLIED SCIENCES
OF
MIDDLE EAST TECHNICAL UNIVERSITY

BY

CAVİT EYÖVGE

IN PARTIAL FULFILLMENT OF THE REQUIREMENTS
FOR
THE DEGREE OF MASTER OF SCIENCE
IN
METALLURGICAL AND MATERIALS ENGINEERING

SEPTEMBER 2017

Approval of the thesis:

DEVELOPMENT OF MAGNESIUM BASED NEGATIVE ELECTRODE MATERIALS FOR NICKEL METAL HYDRIDE BATTERIES

submitted by **CAVİT EYÖVGE** in partial fulfillment of the requirements for the degree of **Master of Science in Metallurgical and Materials Engineering Department, Middle East Technical University** by,

Prof. Dr. Gülbin Dural Ünver _____
Dean, Graduate School of **Natural and Applied Science**

Prof. Dr. C. Hakan Gür _____
Head of Department, **Metallurgical and Materials Engineering**

Prof. Dr. Tayfur Öztürk _____
Supervisor, **Metallurgical and Materials Eng. Dept., METU**

Examining Committee Members:

Prof. Dr. M. Kadri Aydınol _____
Metallurgical and Materials Engineering Dept., METU

Prof. Dr. Tayfur Öztürk _____
Metallurgical and Materials Engineering Dept., METU

Assoc. Prof. Dr. H. Emrah Ünalan _____
Metallurgical and Materials Engineering Dept., METU

Assist. Prof. Dr. Simge Çınar _____
Metallurgical and Materials Engineering Dept., METU

Assist. Prof. Dr. Burak Ülgüt _____
Chemistry Dept., Bilkent University

Date: 06.09.2017

I hereby declare that all information in this document has been obtained and presented in accordance with academic rules and ethical conduct. I also declare that, as required by these rules and conduct, I have fully cited and referenced all material and results that are not original to this work.

Name, Last Name : CAVİT EYÖVGE

Signature :

ABSTRACT

DEVELOPMENT OF MAGNESIUM BASED NEGATIVE ELECTRODE MATERIALS FOR NICKEL METAL HYDRIDE BATTERIES

Eyövge, Cavit

M.Sc., Department of Metallurgical and Materials Engineering

Supervisor: Prof. Dr. Tayfur Öztürk

September 2017, 77 pages

Negative electrode materials of the nickel metal hydride (NiMH) batteries generally based on AB_5 or similar compounds that make use of rare earth elements. The high cost of these elements makes it necessary to look for other alternatives that are more readily available and of low cost. It is also desirable to aim for materials that would have discharge capacity higher than roughly 350 mAh/g, which is typical of AB_5 compounds. Magnesium-based hydrogen storage alloys have attracted considerable attention as an alternative due to their high hydrogen storage capacities. For instance, if Mg alloyed with nickel in the form of Mg_2Ni alloy could be hydrided and dehydrided reversibly at room temperature, could yield discharge capacity in excess of 1000 mAh/g.

Currently, there are two difficulties with Mg-based alloys. The first is their high stability where reversible hydrogenation occurs at temperatures well above room temperature. Nanostructuring via ball milling or similar methods yielded alloys of low stability. The $Mg_{50}Ni_{50}$ composition is of particular interest in this respect. The second difficulty is the durability of Mg alloys in the alkaline environment. Mg-

rich alloys are subject to corrosion in alkaline environments resulting in a fast decay of discharge capacity. The current work deals with $Mg_{50}Ni_{50}$ composition and aims to develop an alloy with an improved electrochemical performance and durability as a negative electrode material.

Mg alloy in this study was synthesized via ball milling of elemental powders; Mg and Ni mixed in equal atomic proportions. This resulted in a mixed structure composed of amorphous $Mg_{50}Ni_{50}$ and nanocrystalline Mg_2Ni. The powder synthesized yielded a discharge capacity of 329 mAh/g in the first cycle; but, was subject to a fast capacity decay down to 50 mAh/g after 20 cycles, caused probably by corrosion of the active metal in an alkaline environment.

So as to obtain a more durable active material, an attempt was made to protect the electrode by surface coating. The electrode was surface coated with nafion, which is known to be permeable H^+ but repulsive to OH^-. This not only reduced the degradation rate of the electrode but also resulted in a significant increase in the discharge capacity of the $Mg_{50}Ni_{50}$. With a 2.80 μm thick nafion coating, the electrode yielded a discharge capacity of 489 mAh/g, an increase by a factor 1.5. This capacity was reduced to 338 mAh/g after 20 cycles.

The beneficial effect of nafion coating was further checked with A_2B_7 alloy, where Mg content is low and therefore of better durability. This has shown that the capacity increase does occur also with A_2B_7 alloy. The results are discussed with regard to the possible origin of capacity increase in both alloys.

Keywords: electrochemical hydrogen storage, Mg-based alloys, $Mg_{50}Ni_{50}$, ball milling, nafion coating, corrosion resistance.

ÖZ

NİKEL METAL HİDRÜR PİLLERİ İÇİN MAGNEZYUM ESASLI NEGATİF ELEKTROT MALZEMELERİNİN GELİŞTİRİLMESİ

Eyövge, Cavit
Yüksek Lisans, Metalurji ve Malzeme Mühendisliği Bölümü
Tez Yöneticisi: Prof. Dr. Tayfur Öztürk
Eylül 2017, 77 sayfa

Nikel metal hidrür (NiMH) pili negatif elektrotları genellikle nadir toprak elementi esaslı alaşımlı malzemelerdir. Bu alaşımlar 350 mAh/g civarında bir deşarj kapasitesi sağlayabilirler. Ancak artan enerji ihtiyacı ile birlikte yeni elektrot malzemelerinin geliştirilmesi gündeme gelmiştir. Yeni elektrot malzemeleri ağırlıkça ve maliyetçe düşük ve kazançlı olmalıdır. Birçok alternatif malzeme grubu içerisinden magnezyum esaslı alaşımlar bu açıdan oldukça dikkat çekici hale gelmiştir. Bu durumun temel sebebi Mg esaslı Mg_2Ni gibi alaşımların oda sıcaklığında dönüşümlü olarak hidrürlendikleri takdirde oldukça yüksek deşarj kapasitesine (1041 mAh/g) sahip olmalarıdır.

Mg esaslı alaşımların kullanımına engel teşkil eden iki temel sorun mevcuttur. Bu sorunlardan ilki Mg ve Mg esaslı alaşım hidrürlerinin yüksek kararlılığıdır. Yüksek hidrür kararlılığı nedeniyle dehidrürlenme reaksiyonu oldukça yüksek sıcaklıklarda gerçekleşebilmektedir. Kararlılığın azaltılması nano yapılandırma ve öğütme gibi yöntemlerle azaltılabilmektedir. Bu açıdan $Mg_{50}Ni_{50}$ alaşım kompozisyonu oldukça dikkat çekicidir. Bir diğer sorun ise Mg esaslı alaşımların bazik ortamdaki düşük

korozyon direncidir. Mg bakımından zengin alaşımlar KOH elektrolit ortamında korozyona uğrayarak deşarj kapasitesinin hızlıca düşmesine neden olurlar.

Mevcut çalışmada $Mg_{50}Ni_{50}$ kompozisyonu kullanılarak NiMH pilleri için geliştirilmiş üstün elektrokimyasal preformansa sahip ve dayanıklı bir negatif elektrot malzemesi üretilmesi amaçlanmıştır. Bu çalışmada $Mg_{50}Ni_{50}$ alaşımı elemental tozların değirmende öğütülmesi yöntemiyle üretilmiştir. Bu amaçla toz haldeki Mg (Alfa Aesar, 99.8%) ve Ni (Alfa Aesar, 99.9%) atomik olarak 1:1 oranında karıştırılmış ve 20 saat süreyle öğütülmüştür. Elde edilen ürün amorf $Mg_{50}Ni_{50}$ ve kristalin Mg_2Ni karışımı olmuştur. Öğütülen tozlardan hazırlanan elektrot elektrokimyasal yöntemlerle test edilmiş ve ilk döngüde 329 mAh/g deşarj kapasitesi elde edilmiştir. Ancak korozyon nedeniyle kapasitede hızlı bir düşüş gözlemlenmiş, deşarj kapasitesi 20 döngü sonrasında 50 mAh/g altında bir seviyeye gerilemiştir.

Korozyonun önüne geçebilmek için H^+ geçirebilen ama OH^- geçirmeyen bir kaplama tabakası oluşturma hedeflenmiştir. Oldukça bilindik bir hidrojen iletkeni olan nafion bu amaçla kullanılmıştır.

Nafion kaplamanın performans üzerindeki etkilerini test etmek amacıyla aynı yöntemle hazırlanan elektrotlar test öncesinde daldırarak kaplama yöntemiyle nafion ile kaplanmıştır. Test edilen elektrotta deşarj kapasitesinin yaklaşık %51 oranında arttığı gözlemlenmiştir. Ancak, kaplamasız elektrottaki kadar ciddi olmasa da kapasite kaybı halen devam etmektedir. 20 döngü sonrasında kapasite 338 mAh/g değerine, başlangıç kapasitesinin %66'sı seviyesine gerilemiştir. Nafion kaplamanın kapasite ve dayanıklılık üzerine etkilerinin araştırılabilmesi açısından aynı kaplama işlemi A_2B_7 alaşımında gerçekleştirilmiştir. Elde edilen sonuçlar alaşımlarda gözelenen deşarj kapasitesinin artışının temeli açısından tartışılmıştır.

Anahtar Kelimeler: elektrokimyasal hidrojen depolama, Mg esaslı alaşımlar, $Mg_{50}Ni_{50}$, öğütme, nafion kaplama, korozyon direnci.

Dedicated to my family…

ACKNOWLEDGEMENTS

This study was financially supported by the Scientific and Technological Research Council of Turkey (TUBITAK) under Grant No. 112M193 and also TUBITAK Support Program 2210-C.

Firstly, I would like to express my greatest thanks to my supervisor Prof. Dr. Tayfur Öztürk for his valuable guidance and support throughout this thesis work. His precious advices inspired me and enlightened my academic vision.

Secondly, I would like to thank to my lab mates Fatih Pişkin, H. Gözde Yıldırım, Doğancan Sarı, Pelin Livan, H. Eda Aysal, Necmi Avcı and earlier members Ezgi Onur Şahin, Burak Aktekin, and Assist. Prof. Dr. Gülhan Çakmak and to my other friends in this department.

I would also want to express my gratitude for my friends Kıvanç Alkan, Sertaç Altınok, Baran Tunç, Ulaş Çepoğlu, Kaan Uslu, Başar Süer, H. Burak Ünsal, Deniz Ceran and Metehan Orhan. These people have the greatest share in provoking me to think out of the box, for each and every aspect of the universe and the life itself.

I would like to appreciate all the efforts, support and willing of my dear mother and father, whom have suffered the same stress and fatigue that I have suffered through the whole of my life. For that reason, I probably would not be able to pay my emotional and material debt for the rest of my life.

Finally, and most importantly, I would like to thank my wife Tutku Sıla Vural Eyövge who spent sleepless nights with and was always my support in the moments when there was no one to answer my queries. Her support, encouragement, quiet patience and unwavering love were undeniably the bedrock upon which the past two years of my life have been built. Her tolerance of my occasional vulgar moods is a testament in itself of her unyielding devotion and love.

TABLE OF CONTENTS

LIST OF TABLES

TABLES

LIST OF FIGURES

FIGURES

CHAPTER 1

INTRODUCTION

1.1 Batteries

Batteries are devices that convert chemical energy into electrical energy. This conversion occurs via oxidation and reduction reactions taking place at electrodes. Electron transfer occurring during these reactions is the source of direct electrical current.

Linden (2004) classifies batteries under two main classes, namely primary and secondary batteries. Primary batteries are the ones that can only be used once due to the irreversibility of the redox reactions taking place. Secondary batteries (also known as rechargeable batteries), on the other hand, can be used, charged and reused for several times. Rechargeability mechanism was explained by Orimo and Fujii (2001) as redox reactions in secondary batteries could be reversed by the application of an external electrical energy, and, by this way the battery is restored to the fully charged state.

1.2 Rechargeable NiMH Batteries

Rechargeable batteries have gained more attention in past few decades due to the increased use of portable electronic devices. These devices include cellular phones, portable computers, video cameras and power tools. Vehicles like buses and automobiles were also started to use rechargeable batteries as a source of energy.

The ideal battery for the applications mentioned above should have high energy density, long life, low cost and low toxicity. One of the best battery chemistries

for such applications is the NiMH battery. NiMH batteries are considered as non-toxic, environmentally friendly and low-cost batteries that are widely used in the consumer electronics. It possesses long cyclic life with respect to the older rechargeable battery chemistries like nickel cadmium, even though their energy density is lower than the lithium ion cells. Comparison of the energy densities of the different rechargeable batteries was made by Tarascon and Armand (2001) and so-called Ragone plot showing both the energy and power densities are provided in Fig. 1.1.

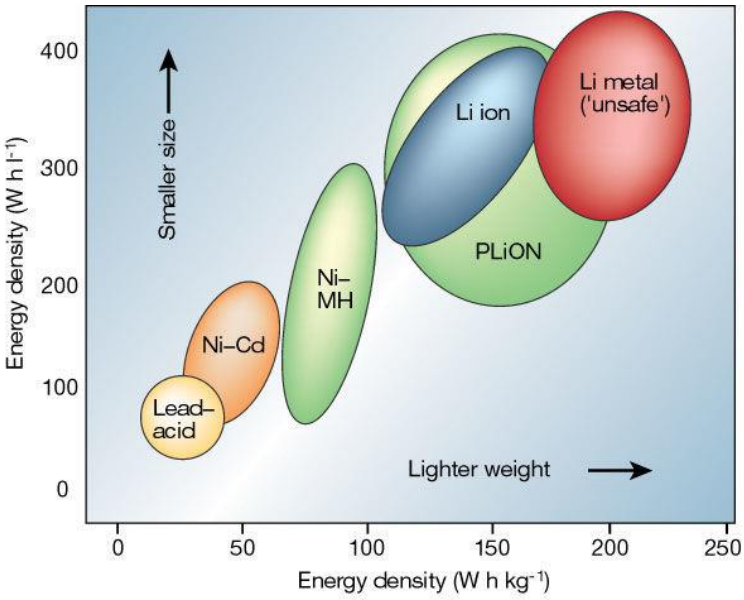

Figure 1.1 *Comparison of the different battery technologies in terms of volumetric and gravimetric energy. Tarascon and Armand (2001).*

Besides their energy density, NiMH batteries have some advantages over other secondary battery types. Their excellent thermal properties, safe use at normal and high voltages and environmentally acceptable electrode materials make NiMH batteries the most suitable one for most of the mobile energy storage applications.

1.3 NiMH Battery Chemistry

NiMH cells have three major components; a negative electrode, a positive electrode and the electrolyte. The positive electrode (or cathode during

discharging) of a NiMH battery generally consists of Co, Zn or Cd-doped nickel hydroxides. The negative electrode, or anode during discharging, is a hydrogen absorbing alloy, which is called as metal hydride. Additives such as Co, Ni or graphite powders are also included the negative electrode similar to the positive electrode to improve electrical conductivity and to provide mechanical strength for compensating volume expansion/contraction during cycling. The electrolyte is generally 6M Potassium Hydroxide solution, which is impregnated into the separators between the electrodes.

Ovshinsky et al. (1993) described the charge/discharge reactions and the corresponding cell potentials with respect to the standard hydrogen electrode of a NiMH battery for negative electrode as:

$$M + H_2O + e^- \underset{discharge}{\overset{charge}{\rightleftharpoons}} MH + OH^- \ (E^0 = +0.49\ V\ vs. SHE) \qquad \textbf{\textit{Equation 1.1}}$$

and, for the positive electrode as:

$$Ni(OH)_2 + OH^- \underset{discharge}{\overset{charge}{\rightleftharpoons}} NiOOH + H_2O + e^- \ (E^0 = -0.83\ V\ vs. SHE) \qquad \textbf{\textit{Equation 1.2}}$$

As a consequence of these reactions, electrolyte quantity does not change during regular cycling. The standard cell potential for a NiMH battery is, therefore, 1.32 V versus SHE.

In a sealed NiMH battery, the capacity is limited by the positive electrode, i.e. the capacity of the negative electrode is larger with respect to the positive electrode (see Fig. 1.2). This provides preserving reactions for the cases where the battery is used in abusive conditions, i.e. over-charge/discharge cases.

If over-charging occurs, water in the electrolyte is electrolyzed and oxygen generation occurs in the positive electrode as:

$$2OH^- \leftrightarrow H_2O + \frac{1}{2}O_2 + 2e^- \qquad \textbf{\textit{Equation 1.3}}$$

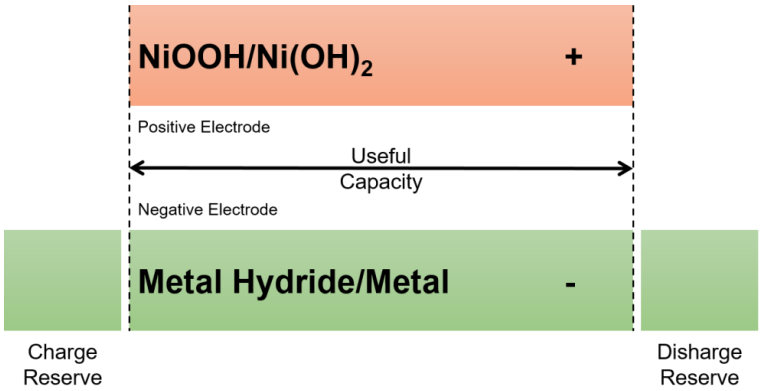

Figure 1.2 *Schematic representation of the NiMH battery electrodes showing the charge/discharge reserves.*

The evolved oxygen diffuses through the negative electrode and combines with hydrogen to form water. It is called as recombination reaction given as following:

$$\frac{1}{2}O_2 + 2MH \leftrightarrow H_2O + 2M \qquad \textbf{\textit{Equation 1.4}}$$

This eliminates the internal pressure build-up if the reaction rate of the recombination reaction is larger than that for oxygen evolution.

During over-discharge, hydrogen is evolved in the positive electrode according to the reaction:

$$H_2O + e^- \leftrightarrow OH^- + \frac{1}{2}H_2 \qquad \textbf{\textit{Equation 1.5}}$$

Generated hydrogen diffuses to the negative electrode and dissociates into the atomic hydrogen by the reaction:

$$M + \frac{1}{2}H_2 \leftrightarrow MH \qquad \textbf{\textit{Equation 1.6}}$$

This is following a charge transfer reaction in which the negative electrode material desorbs hydrogen and creates water as:

$$MH + OH^- \leftrightarrow M + H_2O + 2e^- \qquad \textbf{\textit{Equation 1.7}}$$

As a result, no pressure build-up occurs in the cell. However, according to the Linden (2004), if the over-discharge is prolonged at high currents, then the rate of

the hydrogen recombination reaction with metal cannot exceed the rate of charge transfer reaction; hence, negative electrode starts to discharge deeply. Such a condition damages the battery and causes internal pressure build-up. Therefore, NiMH batteries should not be deeply discharged.

The performance of a NiMH battery is measured in the terms of its capacity, energy density, cycle life and high rate charge/discharge-ability. These properties of the battery are dictated by the electrodes used, which means that the performance of the battery is directly related to the performance of the electrodes. The positive electrode material of NiMH battery, $Ni(OH)_2$, is a well-known and stable material in alkaline environments. The negative electrode, on the other hand, is still the problematic part of the NiMH battery, which degrades in time with the cyclic use in the alkaline environment. Therefore, in order to increase the performance of the NiMH battery, the performance of the negative electrode material should be the primary concern.

CHAPTER 2

LITERATURE REVIEW ON NEGATIVE ELECTRODE MATERIALS FOR NIMH BATTERIES

2.1 Hydrogen Storage Alloys as Negative Electrode Materials

The negative electrode of the NiMH battery should be a hydrogen storage alloy. Metal hydrides, which are formed by a reaction of metal with hydrogen, are used for this purpose. The first definition of the term metal hydride was given by Gibb and Thomas (1948) as "stoichiometric or non-stoichiometric compound in which there is the presence of a metal-to-hydrogen bond". Metal hydrides are similar to the metal in terms of their physical properties. They are generally formed by the reaction of elements from groups IIA-VIIA.

There are several requirements that a metal hydride should satisfy in order to be used in the NiMH battery. Hong (2001) listed these requirements as high electrochemical charge/discharge capacity, good electrochemical catalysis, easy formation, excellent corrosion resistance, suitable hydrogen equilibrium, good kinetics and efficiency, long cycle life and low cost. With the shift of usage area of NiMH batteries from consumer electronics to the hybrid electric vehicles, these requirements are also modified as low self-discharge, good kinetics at low temperature, fast proton diffusion in the bulk, low pulverization rate during service life, and endurance of elevated temperature storage.

Commonly used metal hydrides are classified in terms of their constituent elements including metals in elemental form and BCC type alloys with AB_5 type, AB_2 type, A_2B type and AB type alloys. In the A/B structured alloy formulations, the A component forms the stable hydride, while the B component performs in a

catalytic manner for enhancing hydriding/dehydriding characteristics and improving stability. Sandrock and Thomas (2001) were extensively investigated the properties of the metal hydrides in detail, and the results of their findings are given in Table 2.1.

Table 2.1 *Metallic and intermetallic compounds with their hydrogen storage properties. Sandrock and Thomas (2001).*

Type	Alloy	Hydride	Structure	wt. % H	$P_{eq.}$, T (K)
Elemental	Pd	$PdH_{0.6}$	Fm3m	0.56	0.02 bar @298 K
AB_5	$LaNi_5$	$LaNi_5H_6$	P6/mm	1.37	2 bar @ 298 K
AB_2	ZrV_2	$ZrV_2H_{5.5}$	Fd3m	3.01	10^{-8} bar at 323 K
A_2B	Mg_2Ni	Mg_2NiH_4	P6mmm	3.59	1 bar @ 303 K
AB	FeTi	$FeTiH_2$	Pm3m	1.89	5 bar @ 303 K
BCC	TiV_2	TiV_2H_4	BCC	2.6	10 bar @ 313 K

Among these alloy systems, AB_5 type alloys gathered a lot of attention due to their acceptable hydrogen storage capacity and good kinetics at room temperature. For that reason, NiMH batteries were adopted AB_5 type alloys as negative electrode material for many years. However, with the increasing demand in the mobile energy storage applications, the capacity provided with AB_5 type alloys became insufficient. Hence, studies in the past decade focused on the development of new alloys that have even higher storage capacities.

2.2 Mg and Mg-Based Alloys

Mg-based hydrogen storage alloys are very promising negative electrode materials due to being low cost, lightweight, abundant in earth's crust, and environmentally friendly. There exist several alloy types of Mg alloys with Co, Cu, Ni, Sc and Ti, which can be used for the negative electrode material in NiMH batteries. Among them, Ni-based ones gathered attention in terms of high hydrogen storage capacity.

Two groups of MgNi-based alloys are of particular importance as negative electrode material in NiMH. These are Mg_2Ni and MgNi together with additives that substitute the elements Mg and/or Ni.

Most studies dealing with Mg_2Ni concerns the gas phase hydrogen storage. Reilly and Wiswall, (1968) were the first to study the reaction of hydrogen with Mg_2Ni. Two intermetallic compounds of Mg with Ni were investigated in terms of their gas phase hydrogen storage capacities, and, it was found out that at 350°C and 400 psi pressure $MgNi_2$ did not react with hydrogen, whereas, Mg_2Ni reacted at a temperature of 325°C. The reaction temperature of Mg_2Ni with hydrogen was further decreased to 200°C and pressures as low as 200 psi with further cycling. It was also experimentally shown that Mg_2Ni could absorb and desorb hydrogen up to 2.01 at. % at temperatures above 200°C.

The first electrochemical investigation of Mg_2Ni was carried out by Cui et al. (1995). In this study, Mg_2Ni alloy was cast and pulverized, which gave a very little capacity, 8 mAh/g. Shahcheraghi et al. (2013) synthesized amorphous and nanocrystalline mixture of Mg_2Ni by milling the elemental powders and reported a storage capacity of 15 mAh/g. When they added 5% TiO_2 to Mg and Ni mixture, the capacity was improved to 80 mAh/g. This capacity was however reduced to one-third of this value after 8 cycles. They showed the presence of TiO_2 improves the charge transfer during the discharge process.

Cui et al. (1996) carried out several modifications in Mg_2Ni so as to increase the capacity. A discharge capacity of 126 mAh/g was obtained in Mg_2Ni -10% wt. Ti_2Ni. They stated that the presence of Ti_2Ni improved the electrode reaction rate and, thus, helped to obtain enhancement in the discharge capacity. The cyclic stability; however, was not good as the capacity fall to 10 mAh/g after 10 cycles. Similar decay was also reported by Goo et al. (1999) in which the original capacity of 200 mAh/g was reduced to 40 mAh/g, but when coated by Ni the capacity decay was much less, i.e. 50% loss after 20th cycle. So as to coat the

powders with Ni, Lee et al. (2000) have used a two-step ball milling, first Mg_2Ni was obtained then this was milled with Ni so as to obtain a coated powder.

Anik (2009) synthesized Mg_2Ni by the mechanical alloying and obtained a capacity of 210 mAh/g after 40 h ball milling. They also observed a rapid capacity decay, which was attributed to the formation and thickening of $Mg(OH)_2$ surface layer retarding the hydrogen diffusion across the layer.

Substitutions were made in Mg_2Ni in which the replacement of Mg, and/or Ni, was made mostly in small fractions, in some cases up to even a fraction of 0.5. According to Wang et al. (2016), the substitution of Mg reduces the theoretical storage capacity, but in turn, could increase the hydrogenation reaction rate. On the other hand, Ni substitutions were seemed to increase cyclic stability and corrosion resistance.

Starting with Ni substitution, Woo and Lee (1999) studied $Mg_2Ni_{0.9}M_{0.1}$ (M=Co, Cu and Mn) synthesized via mechanical alloying They produced the electrode by sintering at 480°C. The bare alloy had a very low discharge capacity (40 mAh/g), but this improved to 130, and 120 mAh/g with the addition of Co and Mn respectively. In the case of Cu addition, the capacity was remarkably high, i.e. 350 mAh/g. There was also some improvement in the cyclic stability in that with the alloying addition the decrease in capacity was less. The best performance was again obtained with Cu in which the capacity is reduced to 100 mAh/g after 10 cycles. Similar improvements were also reported by Simičić et al. (2006), with the addition of Cu and V.

Zhang et al. (2011) studied the substitution of Ni with Mn. They produced the alloys by melt spinning in which the substitution was $Mg_2Ni_{1-x}Mn_x$ (x=0, 0.1, 0.2, 0.3, 0.4). Mg_2Ni in as melt-spun form was nanocrystalline while the alloy x=0.4 was partially amorphous implying that Mn facilitates the glass forming ability of the alloy. Mn substitution from 0 to 0.4, the discharge capacity was increased

from 96.5 to 265.3 mAh/g. The cyclic stability of the alloy was also improved from 31.3% to 70.2% at the 20th cycle.

Lee et al. (2000) carried out a similar study with Zr in which $Mg_2Ni_{1-x}Zr_x$ (x=0.1 and 0.3). They have obtained an amorphous Mg_2Ni alloy in which the storage capacity was 400 mAh/g. The addition of Zr for x=0.3 increased storage capacity from 380 mAh/g and x=0.3 to 540 mAh/g. They found, via X-ray photoelectron spectroscopy (XPS), that atomic binding of Mg in amorphous alloys was lower than that at the crystalline one. They argue that this promotes the rate of hydrogen diffusion and charge transfer reaction. However, this improved capacity could not be maintained through cycling which was attributed to the formation of a passive layer of $Mg(OH)_2$.

Improvements obtained with Mg substitutions were not much different than those reported above. Zhang et al. (2007) synthesized the alloy, in which Mg was partially replaced with Zr, $(Mg_{1-x}Zr_x)_2Ni$ (x=0 and 0.1). The synthesized alloy had a maximum discharge capacity of 140 mAh/g and capacity retaining rate for 10 cycles was 72%.

Anik (2009) studied on the substitutions of Al, Zr and Ti with Mg in Mg_2Ni alloy. Alloys synthesized via ball milling from the elemental powders to obtain Mg_2Ni, $Mg_{1.5}Al_{0.5}Ni$, $Mg_{1.5}Zr_{0.5}Ni$, $Mg_{1.5}Ti_{0.5}Ni$. Pure Mg_2Ni gave 258 mAh/g discharge capacity but 10% of this capacity was left after 20 cycles. The highest capacity was attained from $Mg_{1.5}Ti_{0.5}Ni$ with 414 mAh/g. However, the capacity retention rate was not good enough, i.e. only one-third of the capacity was obtained after 20 cycles. Al and Zr substituted alloys did not increase the performance as much as Ti, capacities obtained from these alloys were 166 and 322 mAh/g, respectively. Despite the presence of very low initial discharge capacity, $Mg_{1.5}Al_{0.5}Ni$ alloy kept almost 45% of its initial capacity at 20th cycle.

Zhang et al. (2008) modified Mg_2Ni composition to $Mg_{2-x}Zr_xNi$ (x = 0, 0.15, 0.3, 0.45 and 0.6) by mechanical alloying. When Zr content changed from 0 to 0.6, the

maximum discharge capacity of the alloy milled for 20 h raised from 11.52 to 361.28 mAh/g, and the capacity retaining rate after 10 cycles enhanced from 35% to 89%. For a fixed milling time, the growth of Zr content significantly raised discharge potential of the alloys.

The substitution of Mg with a more electronegative element, like Al or Mn, was studied by Kohno et al. (1996). They found that Mg_2Ni in crystalline form showed nearly 10 mAh/g capacity, while mechanically ground and substituted Mg_2Ni the capacities were much higher. This alloy powder was found to be mainly changed to an amorphous-like state by this treatment. Consequently, the negative electrode of the mechanically ground Mg_2Ni alloy showed a large discharge capacity of 750 mAh/g, which was two and one-half times that of AB_5 type alloys. It was also found that the hydrogen reversibility of the mechanically ground $Mg_{1.9}Al_{0.1}Ni$ alloy electrode remarkably increased. This significant improvement of hydrogen storage properties seemed to be achieved by the increase in the crystal boundary and a heterogeneous strain in this alloy; but, cycling stability needed to be improved. Due to the capacity decay, only 50% of the initial capacity remained after 20 cycles.

Within the same group, i.e. Kohno et al. (1999), mechanical grinding of Mg_2Ni with the addition of Ni or Pd powders was studied. This new alloy powder was found to contain an amorphous-like matrix with dispersed nano Ni or Pd particles. As a result, Mg_2Ni alloy with Ni showed a large discharge capacity (830 mAh/g) which was higher than that of the Al-Mn substituted alloy. With Pd, the cycle life of the alloy electrode was improved considerably, 75% of the initial capacity (600 mAh/g) was preserved after 20 cycles.

Partial substitution of Mg with V and Ni with Al in Mg_2Ni was studied by Luo (1999). The capacities obtained were rather low, the best value was 220 mAh/g in $Mg_{1.9}V_{0.1}Ni_{0.8}Al_{0.2}$.

Based on the review above, it may be concluded that the composition of Mg_2Ni can give its best performance when it is mixed with Ni and gives a capacity of 830 mAh/g. For the increased cyclic stability, Pd added Mg_2Ni can be used with a capacity retention rate of 75%, which gives 600 mAh/g after 20 cycles.

Studies reported above were all based on A_2B composition. An alternative to this would be to switch to AB composition, i.e. $Mg_{50}Ni_{50}$. The first report of this composition was made by Lei et al. (1994). In this study, elemental powders of Mg and Ni were mixed in equal atomic proportions and were milled mechanically yielding an amorphous alloy. A discharge capacity of 380 mAh/g was reported for this alloy. Following this work, Sun et al. (1995) conducted several experiments on alloys $Mg_{50}Ni_{50}$, $Mg_{45}Ni_{55}$ and $Mg_{60}Ni_{40}$. They reported that $Mg_{50}Ni_{50}$ composition had the highest capacity of 390 mAh/g in the first cycle. There was; however, a pronounced capacity decay below 150 mAh/g at 9th cycle. A similar report was published by Liu et al. (2002) which showed 400 mAh/g at the first cycle and reduced to 150 mAh/g after 10 cycles.

Ruggeri et al. (2002) ball milled Mg:Ni (1:1) for different periods of time; 10, 20, 40 and 80 hours. They obtained the highest capacity 522 mAh/g, after 10 h of milling. They claim that extended milling could cause crystallization of amorphous MgNi into nanocrystalline $MgNi_2$ and Mg_2Ni. This was explained as the cause of the lower capacity for powders milled longer than 10 hours.

Abe et al. (2002) followed a different route in synthesizing $Mg_{50}Ni_{50}$. They used Mg_2Ni and Ni mixture and ball milled until the alloy was amorphous. The alloy gave a capacity of 430 mAh/g with a decay characteristic similar to the above. The reason of capacity decay was investigated by cyclic voltammetry. They asserted that $Mg(OH)_2$ formed on the electrode surface did not affect the hydrogen diffusion process; but, affected the process of electron transfer. According to this study, the capacity deterioration is caused by the hydrogen generation reaction on the electrode interface becoming more predominant than the absorption reaction.

Liu et al. (1997) partially substituted Ti for Ni in $Mg_{50}Ni_{50}$ and reported an increase in discharge capacity up to 400 mAh/g and less capacity decay of 66.5% after 9 cycles. The substitution of Zn for Ni showed no effect on the discharge capacity; but, deteriorated the capacity retention. The substitution of Fe, W, Cu, Mn, Cr, Al or C for Ni reduced capacity while the capacity decay was not as pronounced. The substitution of Se, Sb, Co, or Si decreased both the discharge capacity and the cycle life.

Liu et al. (1997) studied on the ternary compositions. Optimum ternary alloys with reasonable discharge capacities and cycle lives were $Mg_{50}Ni_{45}M_5$ (M=Mn, Cu or Fe), with maximum capacities of 345, 343.3 and 273.3 mAh/g, respectively. The capacity decay after 9 cycles was 57.5%, 51.4% and 40.5% in the same order.

In order to improve the cycle life, Han et al. (1999) coated the surface of the amorphous $Mg_{50}Ni_{50}$ alloy with Ti, Al and Zr by ball milling. The first cycle capacity of the uncoated amorphous alloy was 400 mAh/g. Of the coatings evaluated Ti coating was very effective to improve cycle life, i.e. 60% of the initial capacity was preserved after 10 cycles. A similar study was carried out by Jiang and Gasik (2000). In this study, the first cycle capacity of 400 mAh/g was preserved to 65% after 20 cycles with Ti coating. Zr coating was also seemed to be effective, i.e. 57% of the initial capacity could be preserved. However, Al coating did not improve the cyclic stability, capacity reduced below 120 mAh/g. Authors also reported results of quaternary amorphous alloys.

Goo and Lee (2002) investigated diffusivity of hydrogen in the $Mg_{50}Ni_{50}$, Ni being partially replaced by Zr in both crystalline and amorphous form. They reported a discharge capacity of 580 mAh/g for the $Mg_{50}Ni_{43}Zr_7$ alloy in amorphous form. Using chronopotentiometry method they found that the diffusion in amorphous phase was slower ($D=3.97\times10^{-10}$) than that of the crystalline phase ($D=1.29\times10^{-9}$). Moreover, they observed that unlike the crystalline alloys the diffusivities in amorphous phase was strongly dependent on the hydrogen

concentration. Increasing hydrogen content in the amorphous alloy decreased the diffusivity of hydrogen.

The effect of surface modification of amorphous $Mg_{50}Ni_{50}$ by carbon was examined by Abe et al. (2003). In this study, first, the elemental powders were milled to obtain amorphous structure and then they were further milled with carbon for coating purposes. The unmodified $Mg_{50}Ni_{50}$ alloy had a discharge capacity of 400 mAh/g while capacity exceeded 480mAh/g for the carbon modified sample. In addition, the carbon modification improved the cyclic stability of the alloy as compared to the uncoated alloy.

Effect of particle size on capacity and cyclic behavior of amorphous $Mg_{50}Ni_{50}$ was studied by Rongeat and Roué (2004). $Mg_{50}Ni_{50}$ was milled to obtain an amorphous alloy and then sieved into three particle size (d) fractions that are; $d>75$, $20<d<75$ and $d<20\mu m$. They reported discharge capacity values of 439, 396 and 328 mAh/g in the same order, i.e. the capacity was higher for coarse particles. The cycle life was better also with coarse particles. For instance, with 75μm particles, the electrode retained 41% of its initial capacity after 15 cycles. These improvements were attributed to the low specific surface area of the large particles, where $Mg(OH)_2$ is formed. They also asserted that the electrode resistance to pulverization could be improved with large particle size.

Rongeat et al. (2006) investigated several modification methods to enhance the cycle life of the amorphous $Mg_{50}Ni_{50}$ alloy. The methods used were listed as; mechanical coating of particles, like TiO_2, on the alloy, chromate coating by electroless deposition and the addition of chromate salt or NaF into the electrolyte. None of these methods were successful, i.e. the cycle life of the electrodes remained unsatisfactory. Authors have found that the modification of the bulk composition of the MgNi alloy with elements such as Ti and Al was more effective. For instance, a $Mg_{0.90}Ti_{0.10}Ni_{0.95}Al_{0.05}$ electrode retained 67% of its initial discharge capacity (404 mAh/g) after 15 cycles compared to 29% for MgNi. They were able to develop an optimized electrode; $Mg_{45}Ti_5Ni_{47}Al_3$ with a

particle size of d>150 μm, which showed a decay rate as low as 0.2% per cycle when charged to 300 mAh/g.

A study by Shao et al. (2009) covers $Mg_{50}Ni_{50}$ alloy as well as almost all compositions in Mg-Ni system; $Mg_{90}Ni_{10}$, $Mg_{80}Ni_{20}$, $Mg_{67}Ni_{33}$ (Mg_2Ni), $Mg_{60}Ni_{40}$, $Mg_{50}Ni_{50}$, $Mg_{40}N_{60}$, $Mg_{33}Ni_{67}$ ($MgNi_2$) and $Mg_{30}Ni_{70}$. The alloys were prepared by mechanical alloying. $Mg_{60}Ni_{40}$, $Mg_{50}Ni_{50}$, $Mg_{40}N_{60}$ and $Mg_{33}Ni_{67}$ were described to have a "BCC type amorphous" structure; whereas, $Mg_{30}Ni_{70}$ alloy had an "FCC type amorphous" structure. Based on gas phase measurements, the alloy $Mg_{50}Ni_{50}$ was the best in terms of both the capacity (1.85 wt. % hydrogen) and the kinetics at 100°C temperature.

Findings reported above indicate that amorphous Mg-Ni, alloys are possible candidates as the negative electrode materials. The capacity obtained from $Mg_{50}Ni_{50}$ can reach 439 mAh/g without any additional elements and capacity retention rate can be increased to 96% with partial replacement of Mg and Ni with Ti and Al, respectively.

2.3 Surface Modification of Negative Electrode Materials

Rapid corrosion in the alkaline environment of Mg and Mg-based alloys prevents their use as negative electrode materials. This was explained by Wang et al. (2009) as Mg_2Ni and Mg_2NiH_4 are hydrolyzed in both water and alkaline solutions. Spontaneous reaction of Mg_2Ni with water forms $Mg(OH)_2$, Ni and hydrogen. In the case of Mg_2NiH_4, dissociation of Mg_2NiH_4 into Mg_2Ni and hydrogen occurs first, then Mg_2Ni is further hydrolyzed. The hydrolysis characteristics of both Mg_2Ni and Mg_2NiH_4 suggest that they could not be used as negative electrodes in NiMH batteries since sound $Mg(OH)_2$ layer on the electrode surface blocks passage of hydrogen ions into and out of the electrode.

The stability of the hydroxide barrier can be reduced by alloying with different elements. In the study of Yang et al. (2011) doping Mg_2Ni with Ti enhances the corrosion resistance; but, decreases the discharge capacity and kinetics of the

hydriding/dehydriding reaction. Furthermore, application of different fabrication procedures; such as melt-spinning and hydriding combustion synthesis were also found to be effective in terms of improving corrosion resistance and fastening kinetics. Zhang et al. (2011) synthesized Mg_2Ni where Mn was incorporated into the amorphous alloy via melt-spinning technique. They found that Mn addition was quite effective for increased corrosion resistance. However, neither Ti nor Mn addition resulted in the fabrication of Mg_2Ni alloy that could be used in commercial NiMH battery applications.

In the case of $Mg_{50}Ni_{50}$ alloys, the problem is almost the same as these alloys are also subject to degradation. Liu et al. (2002) studied the kinetics of the electrode reaction in an amorphous $Mg_{50}Ni_{50}$ using electrochemical impedance spectroscopy technique. Results showed that the corrosion rate of the electrode is determined by a charge-transfer reaction at the electrode-electrolyte interface. They asserted that the increased charge-transfer resistance was due to the corrosion on the alloy surface.

Distinct types of modifications were introduced to these alloys, such as replacements of Mg and Ni with transition metals or surface treatments. Santos et al. (2007) found that the capacity decay of $Mg_{50}Ni_{50}$ electrodes due to rapid corrosion can be prevented with Cr and Co addition during amorphization. Anik et al. (2011) showed that substitutional replacement of Mg with Ti, Zr and Al for 0.2 at. % could also be beneficial in terms of improving the corrosion resistance. However, these substitutional changes reduce the electrochemical storage capacity; hence no feasible results were obtained especially in terms of the battery applications.

Souza and Ticianelli (2007) have shown that electrochemical coating of $Mg_{50}Ni_{50}$ with metallic elements like Pt and Pd remarkably improves the corrosion resistance in alkaline environments; but, it is only effective in the beginning of cycling. Pt and Pd coated electrodes could preserve capacity at above 300 mAh/g for three cycles, while uncoated electrodes were never reached a capacity value

above 120 mAh/g. Lately, Kim et al. (2013) obtained amorphous/nanocrystalline MgNi composite electrode via hydrogen combustion synthesis and with the help of subsequent ball milling. They coated the electrode with nafion with the result that the capacity was increased 400%, i.e. 713 mAh/g, with respect to the uncoated electrode. This increase in the capacity was attributed to the protection of the electrode from corrosion and progressive film formation of corrosive products in KOH solution due to the nafion coating; however, no information related to the cyclic stability was given.

According to the findings stated above, providing a corrosion resistant surface to the Mg-Ni alloys enhances the capacity dramatically. Providing corrosion resistance via partial elemental replacements may cause reductions in the attainable capacities; but, use of encapsulation methods do not create a negative effect on the capacity. In fact, application of polymeric coatings on these alloys can increase the capacity up to 400%.

2.4 Negative Electrode Characterization

In order metal hydrides to be used in NiMH batteries, they should have good electrochemical performance characteristics such as high discharge capacity, good cyclic stability, good redox reaction reversibility, high rate discharge-ability, low self-discharge rate and ability to tolerate over-charge/discharge conditions. To investigate these properties, electrochemical characterization methods are employed.

2.4.1 Electrochemical Characterization

The electrochemical reactions taking place at the metal hydride electrode in alkaline solution during charging (forward direction) and discharging (backward direction) can be represented as:

$$M + H_2O + e^- \leftrightarrow MH_{ads} + OH^- \qquad \textbf{\textit{Equation 2.1}}$$

$$MH_{ads} \leftrightarrow MH_{abs} \qquad \textbf{\textit{Equation 2.2}}$$

Here, M is the hydrogen storage alloy, MH_{ads} denotes the hydrogen adsorbed on the surface of the metal hydride and MH_{abs} refers to the hydrogen absorbed in the bulk of metal hydride.

The first reaction here is regarded as charge transfer reaction of the negative electrode in which during charging M is reduced to metal MH and a potential of 0.91 V versus Hg/HgO reference electrode should be applied in order this reaction to take place. During discharging, MH is oxidized to the M, inversely. The second reaction indicates that during charging, electrolytically generated hydrogen at the interface of the alloy/electrolyte diffuses into the bulk alloy, and then stores in the metallic lattice in the form of hydride. During the process of discharging, the hydrogen stored in the bulk alloy diffuses toward the surface, where it is oxidized thereafter. Therefore, the electrochemical performance of the negative electrode is related with both the reaction kinetics (charge transfer reaction rate) and the diffusion of hydrogen within the bulk alloy (transformation of MH_{ads} to MH_{abs}).

2.4.1.1 Cyclic Voltammetry

Cyclic voltammetry, by definition, is a technique measuring the potential applied to the working electrode, which is swept at a constant sweep rate and the resulting current measured as a function of potential. Much of the recent interest in electroanalytical chemistry stems from the use of voltammetry to obtain analytical (e.g., concentration), thermodynamic (e.g., redox potentials and equilibrium constants), kinetic (e.g., rate constants for reactions involving electrogenerated species) and mechanistic information about chemical systems in which redox chemistry plays a role. Therefore, CV is an ideal technique for negative electrode electrochemical characterization.

For negative electrode materials, CV was extensively used to determine various properties. A voltammogram similar to that of given in Fig. 2.1 is generally obtained and analyzed for the electrochemical evaluations. In the voltammogram, the x-axis represents the current and y-axis shows the corresponding potentials. Anodic and cathodic peaks represent the discharge and charge potentials for the

electrode being tested. The distance of the peaks from each other and their intensities also give information about the redox reaction reversibility and the corrosion current/potential for the electrode material.

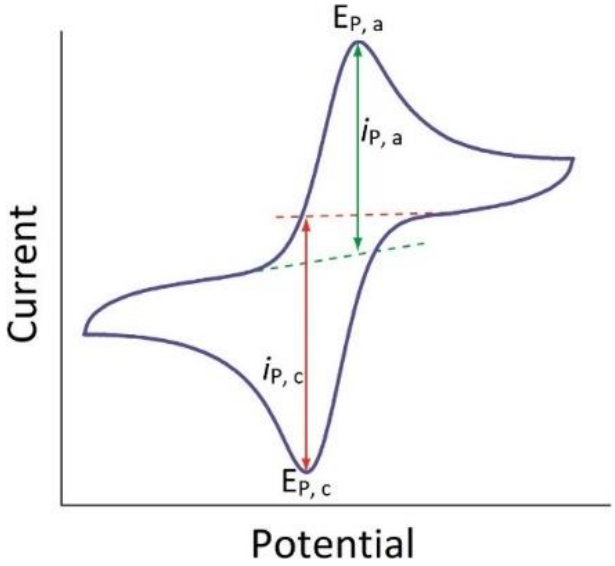

Figure 2.1 *A typical voltammogram from the CV experiment performed on the negative electrode material.*

Gamboa et al. (2002) used this technique in AB_5 type negative electrode material to analyze charge transfer reactions of this alloy. They calculated the effective surface area of the metal hydride electrode, via CV, to be 770 cm^2/g. Li et al. (2006) investigated the effects of electrolyte type on the negative electrode using 7M NaOH as electrolyte instead of KOH. They calculated the Coulombic capacity from the anodic polarization current density and estimated the hydrogen surface coverage capacity by extrapolation of the Coulombic capacity versus inverse scanning rate plots. Hydrogen surface coverage capacity was 0.97 C/g in a KOH electrolyte and 1.69 C/g in a NaOH electrolyte. They concluded that H_2 evolution from the metal surface was obviously suppressed in a NaOH electrolyte compared to a KOH electrolyte.

Uluc et al. (2014) utilized CV to determine hydrogen content on different Pd-Au alloys. They found that the H^+ reduction at the surface of the $Pd_{75}Au_{25}$ alloy is

faster than the $Pd_{95}Au_5$ alloy. They also asserted that peak potential of the CV scans could indicate the strength of the interaction of hydrogen with the surface or bulk.

Etiemble et al. (2013) investigated the influence of Pd addition to Mg-Ni-Ti-Al based negative electrode materials via CV. The results showed that the anodic charge decreases more rapidly with cycling for Pd-modified alloy. Moreover, the open circuit potential (i.e., corrosion potential) was found to be more positive (-0.86 V versus Hg/HgO reference electrode for Pd-modified alloy compared to -0.90 V versus Hg/HgO reference electrode for the unmodified). They claimed via CV that Pd addition improves the oxidation resistance of the electrode in KOH electrolyte.

In the study of Ayari et al. (2015) hydrogen diffusion coefficient in $LaTi_2Cr_4Ni_5$ alloy synthesized via ball milling was investigated. They took several CVs at various scan rates between 10 to 60 μV/s and analyzed anodic peak potentials to calculate diffusion coefficient. Their results showed that hydrogen diffusion coefficients are equal to 4.18×10^{-8} and 7.17×10^{-8} cm^2/s after 8 and 20 h of milled alloys, respectively.

Studies described above shows that CV is a very beneficial technique for electrochemical characterization of negative electrode materials. The data obtained from the voltammogram can be used for the determination of redox reaction taking place at different potentials as well as the calculation of the diffusion coefficient and corrosion resistance of the alloy to be used in the alkaline environment.

2.4.1.2 Galvanostatic Cycling

Galvanostatic cycling or cyclic charge/discharge is an important technique for examining the storage and cycling behavior of electrode materials. The voltage of an electrochemical cell depends on the state of charge or discharge of the electrode materials of the cell. During galvanostatic cycling, a constant current (I)

is applied to the cell and the potential of the cell (V) was monitored as a function of time (t) or state of charge/discharge. The product of the applied current (in ampere) and the time (in hours) for complete hydrogen ion (H^+) removal/insertion is the total charge (in mAh) stored by the material and is termed as the capacity of the electrode material. The capacity obtained per unit mass of the active material is termed as specific capacity, which is defined by;

$$C = \frac{It}{m} \qquad \textbf{\textit{Equation 2.3}}$$

where C is the specific capacity in mAh/g; I is the current applied in mA; t is the time taken for complete discharge/charge in hours and m is the mass of active material in grams. The theoretical specific capacity of an electrode material is given by the following relation;

$$C_{th} = \frac{NF}{3.6M} \qquad \textbf{\textit{Equation 2.4}}$$

where C_{th} is the theoretical specific capacity in mAh/g; F is the Faraday constant (96,496 coulombs per mole) obtained by the product of electronic charge (1.6×10^{-19} C) and Avogadro's number (6.022×10^{23} mol^{-1}); N is the number of H^+ ions/electrons involved in the electrochemical reaction per mole of the electrode material and M is the molar mass of the compound in g/mol.

In literature, there are many studies include galvanostatic cycling as an electrochemical characterization method. For example, Bala et al. (2014) used this method in the examination of Co and Sn modified $LaNi_5$ alloy. Analysis of potential changes on galvanostatic charge/discharge plots showed that hydrogen absorption, and thus, crystal lattice expansion/contraction are prone to substantial surface development. For the tested $LaNi_{4.5}Co_{0.5}Sn_{0.1}$ electrode, a surface increase caused by lattice contraction (hydrogen desorption) was much less intense and it is evident in the first discharge cycle only.

According to Durairajan et al. (2000), electrode cycling released degradation of $LaNi_{4.27}Sn_{0.24}$ particles which manifested itself by further powder material

pulverization and the mean particle size linearly or exponentially decreases with cycle number.

The cycle life of the MgNi based negative electrode materials was evaluated by the attenuation coefficient (k_n) in the study of Santos et al. (2007). Their evaluation was depended on the decay of the curves of discharge capacity as a function of the number of cycles. Concerning the cycle of life of the electrodes of Cr, Co, Ti and V modified MgNi electrodes, they found that the best results were obtained for the Mg-Ni-Cr and Mg-Ni-Co alloys.

Lately, Zhang et al. (2016) evaluated the electrochemical hydrogen storage properties of $MgTiNi_x$ (x = 0.1, 0.5, 1, 2) alloys prepared by ball milling via galvanostatic cycling. Their results indicated that in the ternary alloys with the same atom ratio of Ti and Mg, the number of activation cycles decreases with increasing the Ni content.

Results of the studies given above indicate that galvanostatic cycling is an essential characterization method for negative electrode materials. It gives information about both cyclic stability of the electrode as well as the physical condition after cycling. Information related to the activation behavior can also be obtained via galvanostatic cycling by observing the discharge capacity values from different charge/discharge cycles.

2.4.1.3 Electrochemical Impedance Spectroscopy

Electrochemical impedance spectroscopy is a nondestructive electroanalytical tool used for the evaluation of mechanistic and kinetic information of a wide range of materials like batteries, fuel cells, and corrosion inhibitors. In EIS studies of battery systems, the cell is held at equilibrium at a constant voltage and a small amplitude AC-signal is applied. The response of the system to this perturbation from equilibrium is measured in terms of the amplitude and phase of the resultant current. The frequency of the AC-signal is varied and the impedance of the cell is recorded as a function of frequency. The impedance is represented as a complex

quantity z comprising of “in phase”, Z_{re}, and “out of phase”, Z_{im}, impedances. The plots of imaginary versus real impedance at different frequencies are called Nyquist plots. In order to analyze the data obtained from the EIS, equivalent circuit models are used. This is because the system’s impedance at any given frequency usually depends on more than one element. In equivalent circuit modeling, the electrode is simulated with incorporating the constituent reactions, i.e. hydrogen diffusion, charge transfer reaction, hydrogen migration etc., and the behavior of each element is then described in terms of electrical components like resistors, capacitors, inductors and Warburg diffusion elements.

The total impedance of a cell is the combination of different processes occurring during cycling, namely, diffusion, electron transfer kinetics, charge transfer impedance, bulk impedance, passivating layers, Warburg impedance and intercalation capacitance. The relative contributions of these different processes depend on frequency. The electron transfer kinetics dominates at high to intermediate frequency range (1 MHz - 1 kHz). The diffusion process dominates in the low-frequency range (1 kHz - 5mHz). An example EIS spectrum for the metal hydride electrodes is given in Fig. 2.2 with the equivalent circuit model. In the model, $R_{electrolyte}$ represents electrolyte resistance, $R_{ptcl/ptcl}$ and $C_{ptcl/ptcl}$ represents resistance and conductance due to particle/particle interaction, $R_{ptcl/cllct}$ and $C_{ptcl/cllct}$ represents resistance and conductance due to particle/current collector interaction, R_{ct} shows the charge transfer resistance, C_{dl} shows the double layer capacitance and Z_W stands for Warburg diffusion element.

Due to the valuable information related to the electrode kinetics, EIS is widely used for electrochemical characterization of negative electrode materials. Humana et al. (2012) investigated the effect of particle size of the negative electrode materials on the electrochemical behavior with the EIS. They used AB_5 and AB_2 type alloys in their study and showed that the smallest particle sizes lead to corrosion and a reduction in the active area of the electrode; hence they suggested

that the particle size should be larger than 50 µm in order to avoid active surface area loss.

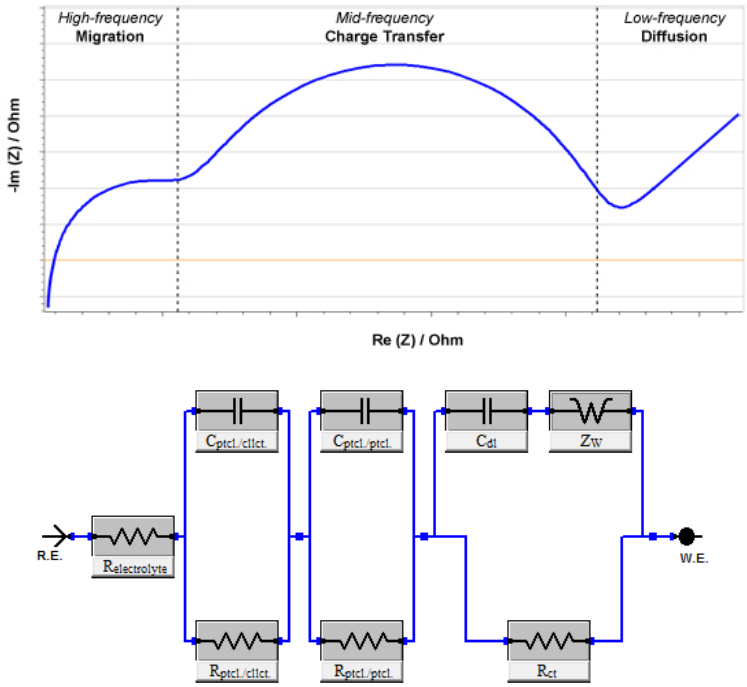

Figure 2.2 *Representative EIS pattern for a negative electrode material of NiMH battery and corresponding equivalent circuit.*

Zhang et al. (2013) performed a study to investigate the rate constants of charging and discharging processes for the negative electrodes via EIS. They proposed a detailed kinetic method based on the energy barrier theory and showed that rate constants of the redox reactions decline with the increase of depth-of-discharge (DOD), which was in agreement with the variations of the hydrogen diffusion coefficient.

In a different approach by Yiwen et al. (2013), electrochemical performance of the AB_5 type negative electrode material in KF added KOH electrolyte was investigated. Using EIS, they calculated the charge transfer resistance of the electrodes in 6M KOH and 0.1M KF-added 6M KOH electrolytes. Their results indicated that charge transfer resistance of the electrode in the KF-free electrolyte

is 20% higher than that for in KF added electrolyte. In other words, KF added to the electrolyte can restrain the corrosion of the alloy particles to some extent.

Kinetic study of the porous negative electrode materials for NiMH batteries was conducted by Lundqvist and Lindbergh (1999). They developed an EIS model based on the physiochemical processes in the electrode and showed that the impedance in the low-frequency region could not be described by an average particle size if the particle size was distributed. They were also able to show that increasing the alloying elements in metal hydride also increases the charge transfer resistance in the porous electrode structures.

Anik (2009) used EIS to observe these mechanisms in Mg_2Ni and MgNi type alloy electrodes prepared by ball milling. In this study, AC impedance spectra measured at various depths of discharges (DODs). The impedance spectra locus changed markedly with DOD for both alloys. At low DODs (0%, 20% and 40% DOD) two distorted capacitive loops at the high and middle frequencies were seen, and a mildly curved line at low frequency in both alloys. The high-frequency capacitive loop was related to the electrode processing due to being independent of DOD or alloy type. The middle frequency capacitive loop was indicated as the charge transfer process at the electrode surface and the low-frequency linear response was reported as the diffusion process. Anik asserted that at low DODs (0%, 20%, 40% DOD) the dehydriding kinetics of the alloys were controlled by both electrochemical charge transfer and hydrogen diffusion, while at 60% DOD and higher, dehydriding kinetics of the alloys were controlled almost totally by the rate of hydrogen diffusion.

Zhang et al. (2011) synthesized nanocrystalline Mg_2Ni type alloy via rapid quenching and investigated the effects of grain size on the electrode behavior. EIS measurements were carried out at 50% DOD for as cast and quenched alloys. They claimed that the electrode kinetics of the as-cast and quenched alloys were determined by a mixed rate-determining process. It was also seen that the radius of the large semicircle in the medium frequency for the Mg_2Ni type alloy shrunk

more with increasing quenching rate. Meaning that the charge transfer reaction is more facilitated at refined grains.

Ni-coated Mg_2Ni electrodes were characterized by Ohara et al. (2013) at 50% DOD. They reported that at the Ni-coated electrode only one semicircle appeared, while there are two semicircles in the bare electrode. This was explained as the hydriding/dehydriding reaction rate of the Mg_2Ni alloys was controlled by hydrogen diffusion.

Above findings indicate that utilization of EIS can give very important information about the charge transfer resistance and the diffusion process for the negative electrode material. In addition to the bare electrode characterization, properties of the coating on the electrode can also be investigated via this method.

CHAPTER 3

SYNTHESIS AND CHARACTERIZATION OF NAFION COATED $Mg_{50}Ni_{50}$ NEGATIVE ELECTRODE MATERIAL

MgNi based alloys seem to be the most suitable candidates for the NiMH battery negative electrode materials due to their high capacity and low cost. However, there are two main problems limiting the use of these alloys as a negative electrode material. The first problem is the chemical stability of the hydrides. MgNi based alloys, when hydrided, requires high temperatures and pressures for dehydrogenation. In order to be able to use these alloys in electrochemical systems, the stability of the hydride should be reduced for reversible hydrogenation/dehydrogenation. Using amorphous forms of MgNi based alloys seem to be an effective solution to overcome this problem since amorphous alloys have enough reactivity/reactive surface to fasten hydrogenation and dehydrogenation kinetics.

The second problem about these alloys is that they are prone to corrosion when used in the alkaline environments. The result of the corrosion is rapid capacity decay, which prohibits the use of these alloys as negative electrode materials. Increasing the corrosion resistance could be achieved via different methods like coating with corrosion-resistant metal or changing the alloy formulae. However, either of the methods showed detrimental effects on the attainable capacity.

Due to the reasons mentioned above, an alloy formula and a suitable coating chemistry are required for MgNi alloys in order to use them in the negative electrode. This study deals with these problems of MgNi alloys. In this study, MgNi based amorphous-like alloys were synthesized and coated with nafion to

prepare a negative electrode for NiMH battery structure. By using amorphous like alloy structure, destabilization of the hydride was aimed and nafion coating was applied to improve the corrosion resistance of the electrode.

3.1 Materials and Methods

Materials used in this study were Mg (Alfa Aesar, -20 +100 mesh, 99.8%) and Ni (Alfa Aesar, -300 mesh, 99.9%). Milling experiment was done via RETSCH planetary mill (PM400 MA Type) with a rotational speed of 400 rpm. A stainless-steel vial with an internal volume of 50 cm^3 was used together with the stainless-steel balls of 10 mm diameter. Ball-to-powder weight ratio was 20:1. Powders were handled under high purity Ar atmosphere using a glove box (MBraun).

Alloys used in electrode preparation was characterized by X-ray diffraction using a Bruker Diffractometer (Cu-Kα). Morphology of the powders was examined with scanning electron microscopy (FEI Nova NanoSEM). The powders were examined by attaching them to double-sided carbon tape.

The electrode prepared with the active powder, when prepared conventionally, was subject to a material loss with cycling. For this reason, a special method was employed in preparing the electrode. Rather than mixing the powders with Ni or Cu powder, the mixing was carried out with thin copper wire. For this purpose, a cable comprising copper wires of 50 μm in diameter were peeled off and the wires were cut at lengths of approx. 10 cm. The wires were then turned into a spherical ball approximately 2 cm in diameter by first bending them and then by hand rolling. Balls produced in this way were typically 2.5 g. Having weighed the ball, it was mixed with the active powder typically 3 g in a plastic container which was shaken randomly so that the powders penetrated into the skeleton of the ball. The ball with integrated active powder was taken out of the container and was placed into an empty container and shaken again so as to remove powders that were loosely connected to the ball. Ball with integrated active powder was cold pressed using a die of 19 mm diameter with a pressure 500 MPa. The pellet obtained was then weighed. Typically, the amount of active powder was 0.25 g. The pellet was

placed into an envelope made by a nickel mesh (100 mesh) of 25×25 mm in size. The envelope was spot welded to a 100-mm long nickel wire of 1.5 mm in diameter used for the connection (see Fig. 3.1).

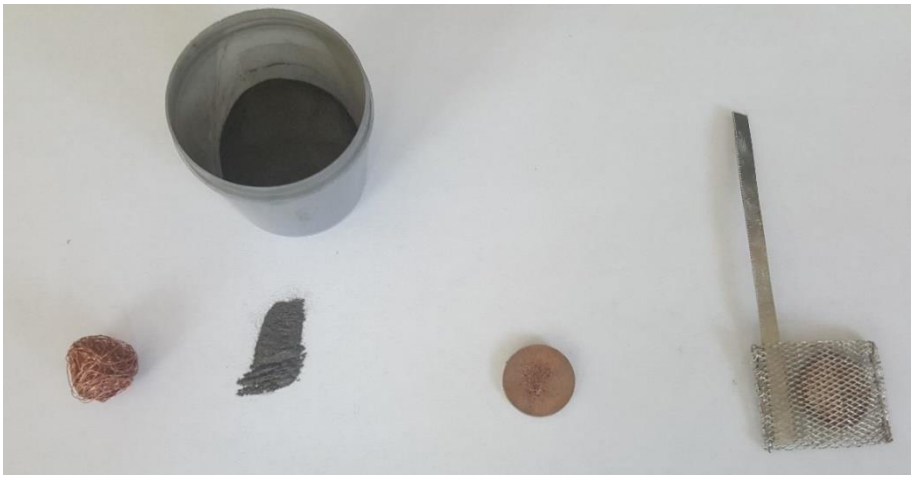

Figure 3.1 *Photograph showing the preparation of electrodes from Cu wire matrix and powders. The prepared electrode is enveloped in a Ni mesh.*

Electrochemical measurements were carried out in a 3-electrode cell as shown in Fig. 3.2. Here the counter electrode was nickel mesh (20 mesh) with a surface area larger than the working electrode. Hg/HgO was used as the reference electrode. The electrolyte was 6M KOH (Sigma-Aldrich, pellets) in distilled water (σ<0.2 μS) solution. All electrochemical experiments were carried out at open atmosphere at 25°C.

Electrochemical measurements were carried using GAMRY Interface 1000 potentiostat/galvanostat. In the CV experiments, electrodes were scanned in the potential range of -0.60 and -1.20 V versus the Hg/HgO with the sweep rate 50 μV/s. EIS measurements were carried out at 0% DOD. An amplitude of 5 mV was applied in the whole frequency range from 10 kHz to 10 mHz. The electrodes were kept at the open circuit potential during the impedance measurements so that the net DC current was approximately zero.

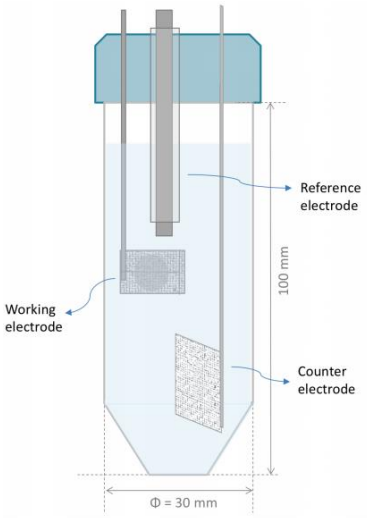

Figure 3.2 *Three electrode cell structure used in the electrochemical tests.*

Perfluorosulfonic acid/Tetrafluoroethylene copolymer (nafion) used for coating was obtained from Ion-Power (LQ-1115-1100 EW). This was in the form of 15 wt. % nafion (i.e. solution in water and isopropanol (with the ratio of 1:2 in the respective order). The solution as supplied was further diluted by adding isopropanol so that the content was reduced to 5 wt. % nafion.

Nafion solution was applied to the electrode via dip coating method. In this method, the electrode was dipped into the 5 wt. % nafion solution and kept there for 2 minutes and then it was slowly removed from the solution. The electrode was then placed in an oven and dried for 1 hour at 100°C. The process was repeated 4 times to obtain a coating layer with a thickness of 2.80±0.09 μm on the electrode.

3.2 Results and Discussions

3.2.1 Structural Characterization

To obtain $Mg_{50}Ni_{50}$ alloy, elemental powders of Mg and Ni were mixed in the atomic ratio of 1:1 in a glove box and placed in a vial. They were milled for durations of 5, 10 and 20 hours.

XRD patterns of milled samples are shown in Fig. 3.3. It is seen that with 5 h milling the pattern is already affected as there is the formation of intermetallic Mg_2Ni, together with peaks of both Mg and Ni. It should be noted that after 10 hours of milling a broad peak centered on approximately 41°, which governs $Mg_{50}Ni_{50}$ amorphous phase, is evident together with Mg_2Ni. Of the metallic peaks, only Ni is discernible. After 20 hours of milling, no metallic peaks are detectable, the whole spectrum is made up of two broad peaks one centered on 41° standing for $Mg_{50}Ni_{50}$ and the other at 44° for Mg_2Ni which has also broadened quite substantially. This sample is designated as $Mg_{50}Ni_{50}$. This is despite the fact that a certain fraction of this sample is Mg_2Ni phase.

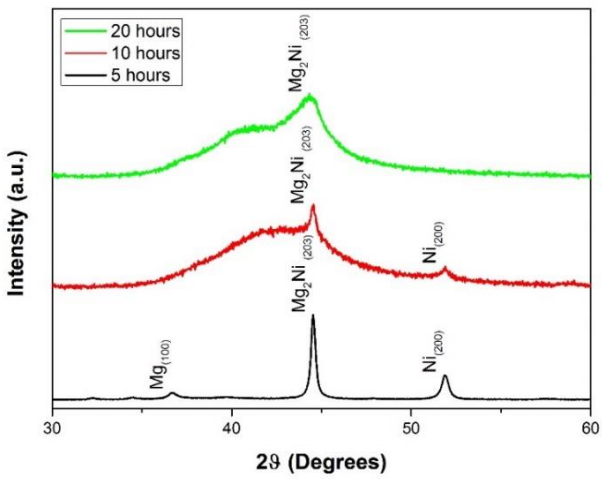

Figure 3.3 *XRD spectra obtain from milled alloys for durations of 5, 10 and 20 hours.*

SEM micrograph of representative powder for 20 hours milling is given in Fig. 3.4. Here, it is seen that the powders were quite irregular in shape and agglomerated. This was a natural consequence of mechanical milling in which repeated cold welding and fragmentation of the powders occur during the processing.

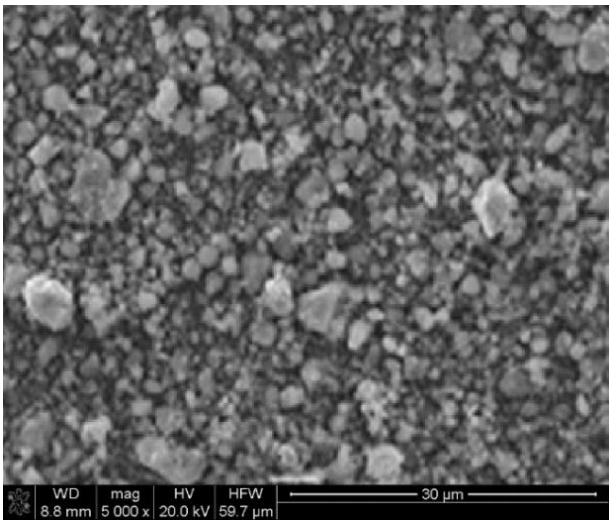

Figure 3.4 *SEM image of the 20 hours milled powders.*

3.2.2 Electrochemical Performance of the Bare Electrode

A typical CV for $Mg_{50}Ni_{50}$ electrode is given at Fig. 3.5. The voltammogram shows two peaks in cathodic and anodic branches.

In the cathodic branch of the voltammogram, a peak is observed at a potential around -1.08 V versus Hg/HgO reference electrode. This part is associated with the adsorption of hydrogen atoms on the electrode surface according to the reaction:

$$H_2O + M + e^- \leftrightarrow MH_{ads} + OH^- \qquad \textbf{\textit{Equation 3.1}}$$

The tail to the left in is attributed to hydrogen evolution at the electrode surface as:

$$H_2O + e^- \leftrightarrow \frac{1}{2}H_2 + OH^- \qquad \textbf{\textit{Equation 3.2}}$$

In the anodic branch, a peak is observed at around -0.81 V versus Hg/HgO reference electrode, which is associated with desorption of hydrogen atoms from the electrode surface as:

$$MH_{ads} + OH^- \leftrightarrow M + H_2O + e^- \qquad \textbf{\textit{Equation 3.3}}$$

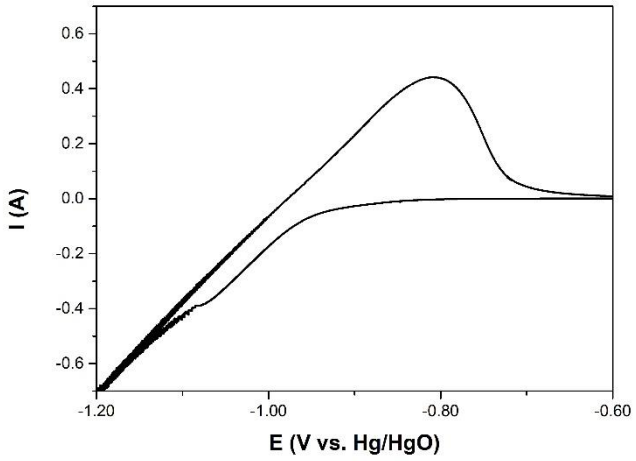

Figure 3.5 *CV of the bare $Mg_{50}Ni_{50}$ electrode showing the potentials of anodic and cathodic reactions.*

A charge/discharge curve recorded for the electrode in the first cycle is given in Fig. 3.6. During charging, the voltage rapidly moves to -1.07 V versus Hg/HgO and thereafter remains almost constant until the electrode is fully charged. The electrode yields a discharge capacity of 329 mAh/g was obtained in the first cycle.

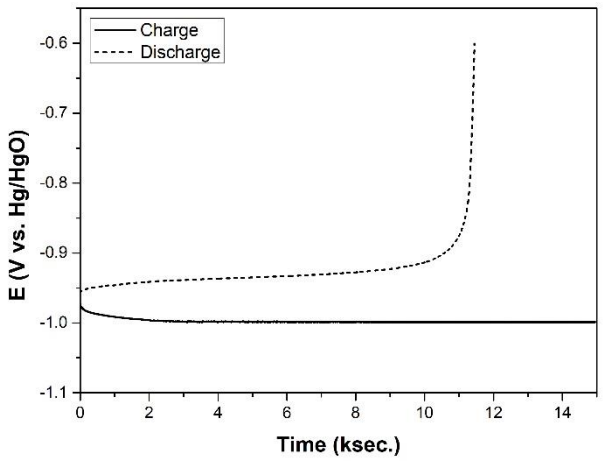

Figure 3.6 *First cycle charge and discharge curves of the bare $Mg_{50}Ni_{50}$ electrode, solid line showing the charge step and short dashed line showing the discharge step.*

The discharge capacity of the electrode in galvanostatic cycling is given in Fig. 3.7. As seen in the curve there is a fast capacity decay in the $Mg_{50}Ni_{50}$ electrode. The capacity which had a value of 329 mAh/g in the first cycle was reduced to 180 mAh/g and 100 mAh/g after 5 and 10 cycles, respectively.

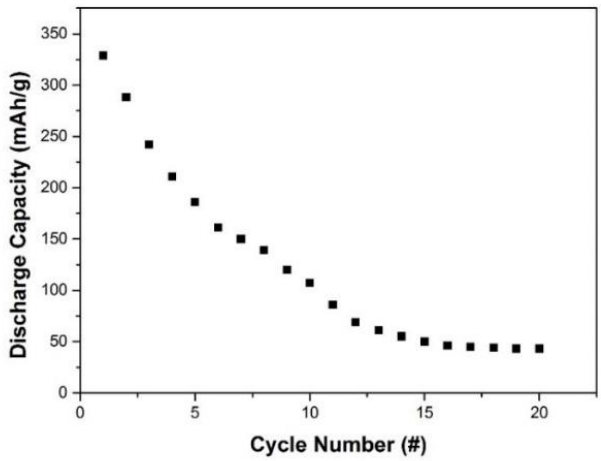

Figure 3.7 *Variation of discharge capacity of bare $Mg_{50}Ni_{50}$ electrode with cycling.*

EIS measurements were used to characterize the surface state of the electrode at fully charged (0% DOD) state. The typical Nyquist plot of the $Mg_{50}Ni_{50}$ electrode is given in Fig. 3.8. Here, though not directly visible, Nyquist plot comprises two semicircular arcs at high and medium frequencies and a line at low frequencies. The first semicircle in the high-frequency region is normally related to the particle-current collector interactions. The second semicircle in the loci are due to the charge transfer processes at the electrode/electrolyte interface, which occurs via:

$$H_2O + M + e^- \leftrightarrow MH_{ads} + OH^- \qquad \textbf{Equation 3.4}$$

The linear part seen in the loci is attributed to mass transfer effect, called as Warburg impedance, which relates to the diffusion of H^+ in the alloy.

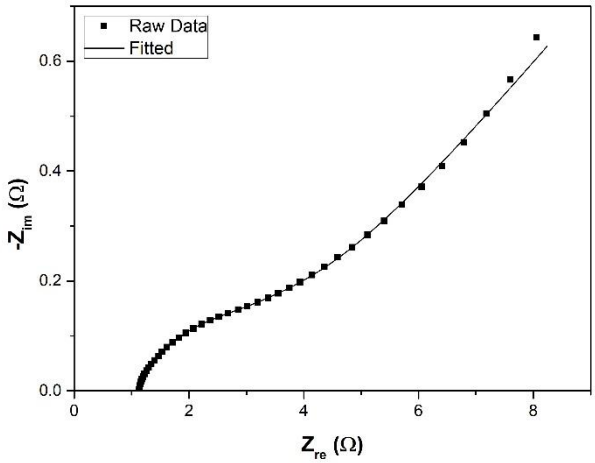

Figure 3.8 *EIS plot of the electrode at fully charged (0% DOD) state, in which the raw data was shown as dots and the fitted data with an equivalent circuit (given in Fig. 2.2) was shown as a line.*

An EIS responses similar to the one obtained in this study was also reported by Liu et al. (2011) for Mg_2Ni, though in their data mid frequency semicircle was better defined. The impedance spectra recorded in the electrode was analyzed using an equivalent circuit model given by Liu et al. (2011) as explained in Chapter 2.4.

Using GAMRY EChem EIS analysis tool, the proposed model matches the obtained data as shown in Fig. 3. 8. This yields a charge transfer resistance of 4.62±0.16 Ω when the electrode is fully charged. This value is rather high considering that the value in Mg_2Ni in the study of Hapçı Ağaoğlu & Orhan (2017) and that in A_2B_7 (see Chapter 4) had values of 0.48 Ω and 1.02 Ω respectively.

3.2.3 Electrochemical Performance of Nafion Coated Electrode

Experiments reported above were repeated with the nafion coated electrodes. CV of the electrode coated with 2.80±0.09 μm nafion is plotted in Fig. 3.9. Here voltammogram of the bare electrode is also shown. It should be noted that there is a shift of voltammogram towards more negative values. For instance, the anodic

peak which occurred at -0.81 V versus Hg/HgO was shifted to -0.84 V versus Hg/HgO with nafion coating.

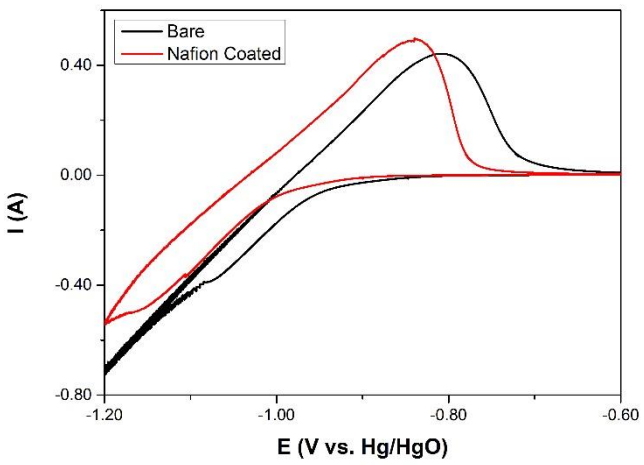

Figure 3.9 *CVs of bare and nafion coated $Mg_{50}Ni_{50}$ negative electrodes, showing the shift of the peak potentials to the more negative values for nafion coated electrode.*

Potential versus time diagram for the first charge/discharge cycle is given in Fig. 3.10. for the bare and nafion coated electrodes. Superimposed on this graph is the curves recorded for the bare electrode. Nafion coated electrode yields a discharge capacity of 498 mAh/g in its first cycle, which is significantly higher than that bare electrode which was 329 mAh/g.

Other than the obtained capacities, there exists another difference in the first cycles of the bare and nafion coated electrodes. In galvanostatic charging, the voltage which initially starts at -1.04 V versus Hg/HgO quickly moves to -1.07 V versus Hg/HgO for the bare electrode. This is slightly different in nafion coated electrode, where the increase in the voltage is more gradual, and, reaches a plateau value only when the electrode is half charged.

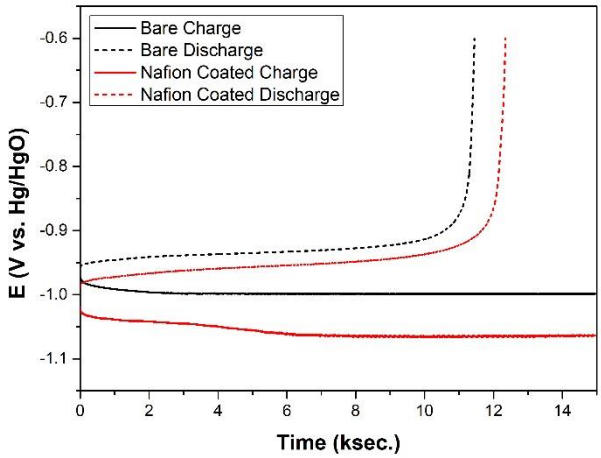

Figure 3.10 *Galvanostatic charge and discharge curves of the bare and nafion coated electrodes showing the deviation of potential during charging and discharging.*

Fig. 3.11 shows the variation of discharge capacity with cycling. It is seen that there is, as before, a capacity decay with cycling, but it is not as pronounced. Data with the bare electrode is replotted on the same diagram. It is clear that the capacity curve with nafion coating has been displaced upwards showing a considerable increase in the discharge capacity. After 20th cycle, the discharge capacity remains at 387 mAh/g. This is significantly more than what was obtained with the bare electrode (50 mAh/g).

EIS responses recorded in fully charged (0% DOD) electrodes after 5 cycles are shown in Fig 3.12. EIS response shows quite a large arc in the medium frequency. Using the same model as above, the analysis yields a charge transfer resistance (R_{ct}) of 8.87±0.68 Ω. This value should be compared with 4.62±0.16 Ω obtained with the bare electrode. This implies that charge transfer resistance has increased substantially with nafion coating.

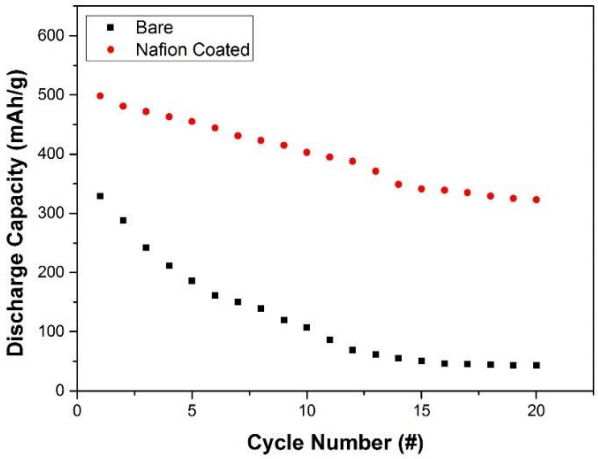

Figure 3.11 *Galvanostatic cycling performance of the bare and 2.80 µm nafion coated electrodes for 20 cycles.*

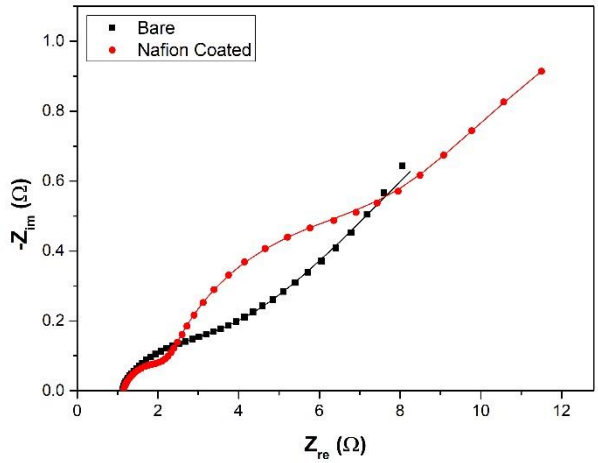

Figure 3.12 *EIS patterns of the bare and nafion coated electrodes obtained within the 10 kHz-10mHz regions.*

It may be stated that nafion coating leads to several alterations in the electrochemical response of $Mg_{50}Ni_{50}$ electrode material. One is that electrode is charged at higher potentials the same is also true for discharge. The reason for how nafion brings about this effect could not be clarified at this stage.

The second important observation is that with nafion coating charge transfer to the electrode becomes more difficult. Surface coating with copper and nickel is quite common in the negative electrode material. Such coatings; however, as shown by Sakai et al. (1991) in Cu coating of AB_5 alloy and by Ohara et al. (2013) in Ni coating of Mg_2Ni alloy has the opposite effect of reducing the charge transfer resistance of the electrode. The only report on how the charge transfer was affected by nafion was reported by Brett et al. (2001) for glassy carbon electrodes where there was also an increase in the charge transfer resistance. They explained this as nafion being less conductive.

The increase of R_{ct} with nafion coating is probably the expected result as there are two charge transfer processes in the case of nafion coated electrode. Since there are two interfaces for the charge transfer; one is the transfer of H^+ to the nafion across the electrode/nafion interface and the other transfer of H^+ from nafion to the electrolyte. It is obvious that these processes are more difficult than a direct transfer of H^+ to the bare alloy surface.

Another important observation is the capacity decay, which occurred both in the bare and nafion coated electrodes. Part of the capacity decay is due to particle drop out. Measuring the weight of the electrode after 20th cycle, the weight loss was determined to be 96 mg for the bare electrode and 53 mg for nafion coated electrode. Correcting the capacity versus cycle curve for this amount by distributing the total mass lost equally into each cycle, it appears that the real capacity decay is slightly less than those reported in Fig. 3.11. Fig 3.13 shows the corrected curve taking particle drop out into account. The values at 20th cycles were calculated with the drop-out measured experimentally. The values at previous cycles were determined by distributing the particle loss equally across the cycling.

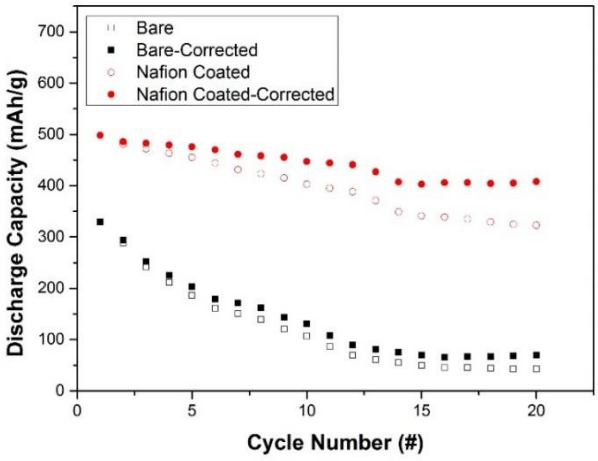

Figure 3.13 *Corrected discharge capacities of the bare and nafion coated electrodes taking mass change into account.*

The corrected capacity values showed that approximately 1/5th of the initial capacity could only be preserved in the bare electrode. Since this value is already corrected for the particle drop out, this reduction in capacity is simply because of the electrode decay during cycling. Thus, corrosion of the active particles may be the major factor of capacity decay for the bare electrode.

For nafion coated electrode, the capacity remaining in the electrode is nearly 82% of the initial capacity. This value is significantly higher than that of the bare electrode. It appears that nafion do protect the $Mg_{50}Ni_{50}$ electrode against corrosion in the alkaline environment. Normally nafion coating would also be expected to prevent particle drop out by forming a protective envelope around the electrode. The fact that there is still particle dropout is a sign that the coating process was less than perfect. This also implies that not all parts of the electrode were fully protected by nafion.

Perhaps the most important observation made in the current work is the increase of discharge capacity that occurs upon nafion coating. Considering the first cycle, the increase is quite significant, i.e. 489 mAh/g as opposed to 329 mAh/g. The only study that measured discharge capacity with nafion coating is that of Kim et

al. (2013). In this study Mg_2Ni which was produced via self-propagating high-temperature synthesis displayed a discharge capacity of 713 mAh/g. This was 4 times the discharge capacity measured at the bare electrode. No explanation was given as to how this increase was obtained, probably due to the fact that the expected capacity in Mg_2Ni is even higher than what they obtained with nafion coating, i.e. 1041 mAh/g.

The analysis of the effect of nafion coating on Mg-based alloys is quite complicated because there is corrosion as well as particle drop out which makes the interpretation quite difficult. For this reason, it might be useful to investigate how nafion coating affects the electrochemical performance of a much simpler system. This is the subject of Chapter 4, where the electrode material is A_2B_7 which is known to be stable in the alkaline environment.

CHAPTER 4

STRUCTURAL AND ELECTROCHEMICAL CHARACTERIZATION OF NAFION COATED A2B7 ELECTRODE MATERIAL

In the previous chapter, effects of nafion coating on $Mg_{50}Ni_{50}$ electrode material were investigated. It was observed that nafion coating increases the discharge capacity of the electrode quite significantly. However, the analysis of this effect was complicated due to the fact that $Mg_{50}Ni_{50}$ is subject to corrosion in an alkaline environment. For this reason, the effect of nafion coating on the electrochemical performance of negative electrode material was investigated in a system, where it is known that electrode is not significantly affected by the alkaline environment.

4.1 Materials and Methods

The material selected for this study is A_2B_7 where the amount of Mg is quite small. EDS analysis of A_2B_7 powder is given in Table 4.1. According to the analysis, the powder has a composition of $(La_{0,70}Mg_{0.30})_2(Ni_{0.85}Co_{0,15})_7$. Crystal structure of powders together with phases present was analyzed with X-ray diffraction using Bruker Diffractometer (Cu-Kα). The XRD pattern obtained was analyzed with Rietveld refinement using the software MAUD (Lutterotti (2000)). Morphology of the powders and compacts were examined with FEI Nova NanoSEM operated at 10 kV. The powder samples were examined by attaching them to double-sided carbon tape.

Electrodes were prepared using the same procedure used in the previous chapter. However, A_2B_7 powders were larger in size than $Mg_{50}Ni_{50}$ which facilitated the electrode preparation. Nafion coating of the electrode made use of the procedure

described in Chapter 3.1. Electrochemical measurements were carried out in a 3-electrode cell structure with details the same as those depicted in Chapter 3.1.

Table 4.1 *Results of the EDS analysis for A_2B_7 powder showing the wt. and at. % distribution of the constituent elements.*

Element	wt. %	at. %
La	34.09	17.20
Mg	2.45	7.07
Ni	54.04	64.53
Co	9.42	11.20

4.2 Results and Discussions

4.2.1 Structural Characterization

A representative SEM micrograph of the powders is given in Fig. 4.1 Here, it is seen that the powders are quite angular in shape with pointed edges probably arising from crushing of the as-produced alloy. XRD pattern obtained from this powder is given in Fig 4.2. Here, the A_2B_7 powder composed of three phases, namely $(La, Mg)_5(Ni, Co)_{19}$, $(La, Mg)_2(Ni, Co)_7$, and $LaNi_5$ hexagonal phases. The weight fraction of phases as determined with Rietveld refinement is given in Table 4.2.

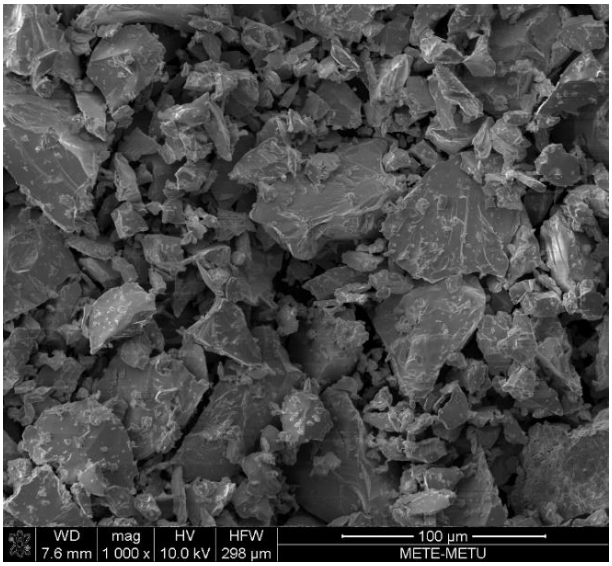

Figure 4.1 *SEM image of A_2B_7 powder showing the general shape and size of the particles.*

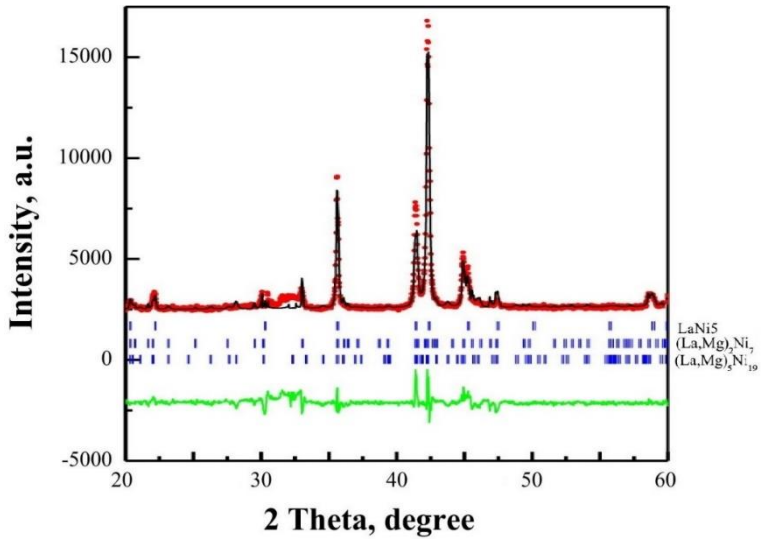

Figure 4.2 *XRD spectrum of the A_2B_7 powder showing the different structure types.*

Table 4.2 *Phase analysis according to the structures obtained via Rietveld refinement.*

Phases	Weight Fraction (%)
A_2B_7	55.3
AB_5	8.6
A_5B_{19}	36.1

4.2.2 Electrochemical Performance of the Bare and Nafion Coated Electrodes

CV of the electrode coated with 2.80±0.09 µm nafion is plotted in Fig. 4.3. Here, voltammogram of the bare electrode is also shown. It should be noted that there is a shift in the voltammogram.

It is interesting that the shift of the voltammogram in the A_2B_7 alloy is different than that $Mg_{50}Ni_{50}$ showed. Here, nafion coated electrode has an anodic peak potential located at -0.85 V versus Hg/HgO. The anodic peak of nafion coated electrode was shifted to less negative potentials with respect to the bare electrode by a value of 0.03 V.

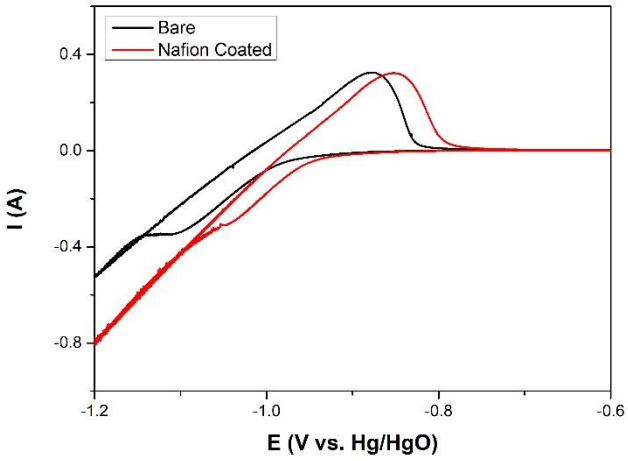

Figure 4.3 *CVs of bare and nafion coated A_2B_7 negative electrodes, showing the shift of the peak potentials to the less negative values for nafion coated electrode.*

CVs of $Mg_{50}Ni_{50}$ and A_2B_7, electrodes both in bare and nafion coated forms are superimposed in Fig. 4.4 (a) and (b). It should be noted that nafion coated electrodes have very similar voltammograms. This means that shifts that have been reported so far relate to the bare electrodes, i.e. nafion coated electrodes have "the same" CV, but observed shifts are due to $Mg_{50}Ni_{50}$ and A_2B_7 in bare forms.

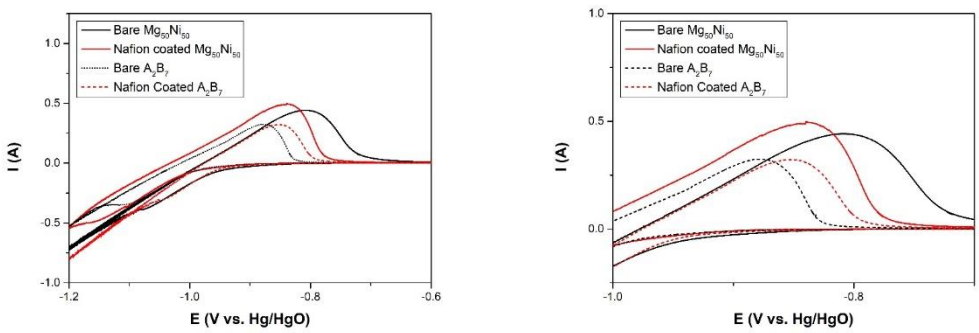

(a) (b)

Figure 4.4 *CVs of $Mg_{50}Ni_{50}$ and A_2B_7 electrodes showing (a) both in bare and nafion coated forms replotted on the same potential vs. current axes and (b) focused window on the anodic potentials.*

Fig. 4.5 shows potential versus time diagram for the first cycle. Superimposed on this graph is the curves recorded for the bare electrode. The coated electrode

yields a discharge capacity of 318 mAh/g. This value is higher than what was obtained from the bare alloy, 230 mAh/g.

It should be noted that there exists another difference in the first cycles of the bare and nafion coated electrodes. In galvanostatic charging, the potential which initially starts at -1.09 V versus Hg/HgO quickly moves to -1.12 V versus Hg/HgO for the bare electrode. This is slightly different in nafion coated electrode where the change in the voltage is more gradual and reaches a plateau value at -1.06 V versus Hg/HgO only when the electrode is charged for half of its capacity. Moreover, nafion coated electrode is charged and discharged at less negative potentials with respect to the bare electrodes as seen in Fig. 4.5. This is a consistent with the voltammogram reported in Fig. 4.3.

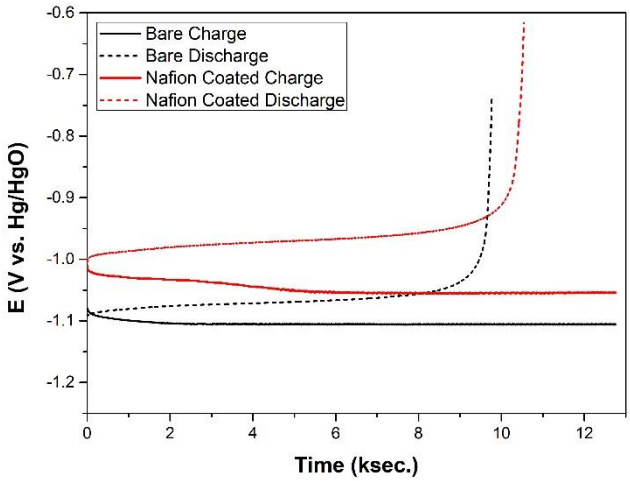

Figure 4.5 *Variation of cell potential with respect to time during charging and discharging for the bare and nafion coated electrodes.*

Fig. 4.6 shows the variation of discharge capacity with cycling. It is seen that the capacity increases with cycling. A total of 5 cycles seems to be enough to fully activate the electrode. Nafion coated electrode after full activation yields a discharge capacity of 449 mAh/g. The data obtained with the bare electrode is replotted on this graph. It is obvious that nafion coated electrode yields a

discharge capacity, which is significantly higher than that of the bare electrode. The full discharge capacity in the bare electrode was 329 mAh/g.

EIS measurement carried out on fully charged (0% DOD) electrodes in the bare and nafion coated forms are shown plotted in Fig. 4.7. The nafion coated electrode shows quite a large arc in the medium frequency as compared to the bare electrode. Using the same model as used in Chapter 3, impedance spectrum yields an R_{ct} value of 5.49±0.98 Ω. This value should be compared with 1.02±0.27 Ω obtained in the bare electrode.

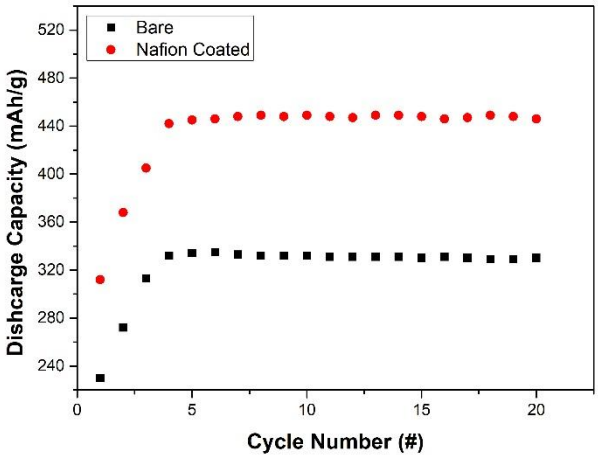

Figure 4.6 *Galvanostatic cycling performance of the bare and 2.80 µm nafion coated electrodes in 20 cycles.*

It should be mentioned that R_{ct} of nafion coated electrode is not similar to coatings that are typically applied to metal hydrides; e.g. Ni, Cu. For instance, Ohara et al. (2013) reported an R_{ct} value of 1.06 Ω, when the electrode was coated with Ni, while the bare electrode yields an R_{ct} of 1.66 Ω. Similarly, Chen et al. (2015) reported a much lower value of R_{ct} with the nano-Ni coating (0.18 Ω) . It is obvious that nafion coating has the opposite effect of increasing the charge resistance and its use may only be justified if it brings other benefits.

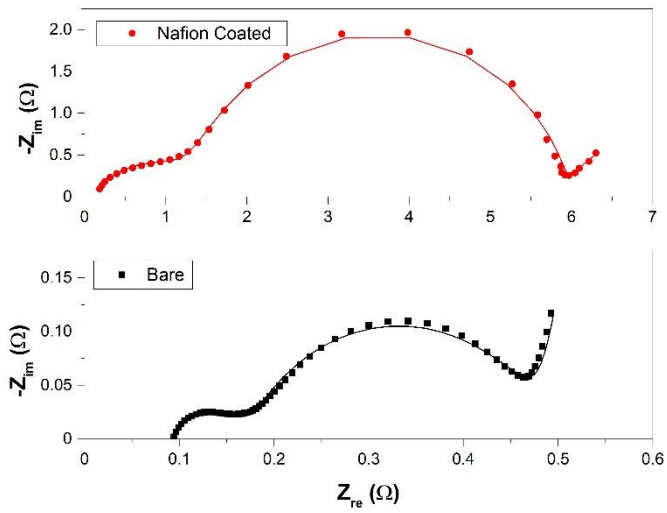

Figure 4.7 *EIS of the bare and nafion coated A_2B_7 electrodes at fully charged states.*

The most striking observation of the current is that nafion coating increases the discharge capacity of the electrodes. This increase can be observed starting from the first cycle, and become more dominant in the subsequent cycles for the $Mg_{50}Ni_{50}$. For the case of A_2B_7 electrodes, again, there exists a large capacity difference in the first cycles of the bare and nafion coated electrodes, and, this difference is preserved in the subsequent cycles.

In order to investigate the origin of the capacity increase, two separate experiments were carried out. In one, the thickness of the nafion was reduced so as to see if the capacity increase was related to the quantity of nafion used. In the other, nafion thickness was kept the same, i.e. 2.80±0.09 μm, but amount of active material in the electrodes was increased so as to check if the capacity increase was a surface related phenomenon.

A total of 4 samples were tested each with a different nafion thickness; bare, 0.70±0.05 μm, 1.40±0.06 μm and the original sample that had a thickness of 2.80±0.09 μm. The discharge capacities measured in the galvanostatic cycling of these samples are given in Fig. 4.8.

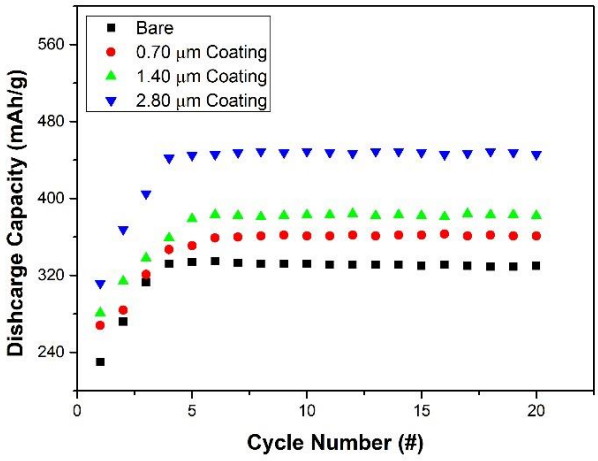

Figure 4.8 *Galvanostatic cycling capacity results from the bare and nafion coated electrodes.*

It should be noted that there is an increase in discharge capacity of the electrode with increasing nafion thickness. The plateau discharge capacity as a function of nafion thickness measured for the samples are shown plotted in Fig. 4.9. It should be noted there is a linear relationship between the two, i.e. the thicker the nafion the higher is the capacity, Table 4.3.

Table 4.3 *Average capacity values of nafion coated electrodes having different coating thickness.*

Electrode	Average Capacity (mAh/g)
0.70 μm thick nafion coated	362
1.40 μm thick nafion coated	383
2.80 μm thick nafion coated	449

It should also be noted that in both bare and nafion coated electrodes the saturation capacity was reached within the first 5 cycles. This indicates that nafion coating does not change the activation behavior of the electrode. In addition, electrode integrity was also maintained in the coated electrode, hence neither capacity nor particle drop was observed.

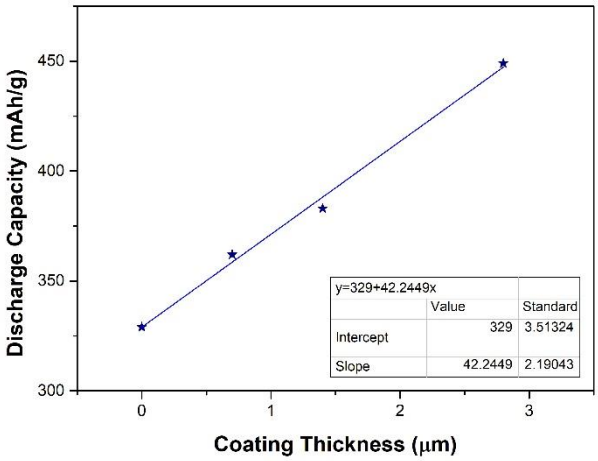

Figure 4.9 *Discharge capacity of the electrodes as a function of the thickness of the nafion coating.*

To check if the capacity increase was a surface related phenomenon, the thickness of nafion coating was kept the same (2.80±0.09 μm), but the amount of active material in the electrode was modified. In the original sample, the amount of active material was 0.25 g. In the new sample, this amount was nearly tripled to 0.68 g. Fig. 4.10 shows the capacity of the electrode measured with different active materials without normalization with respect to the amount used. It should be noted that the discharge capacity is nearly tripled when the active material was tripled, i.e. the discharge capacity normalized per unit mass are the same.

It is obvious from the above experiments that it is the active material that stores the charge. The other possibility was that nafion itself may act as a hydrogen storage medium. Although this possibility was ruled out by the above experiment, a further check was carried out. For this purpose, bare nickel mesh was nafion coated to a thickness of 2.80±0.09 μm. CV of this sample is given in Fig 4.11 together with the CV of bare Ni. There are no oxidation-reduction peaks observed in the spectrum and that both curves are almost identical. This implies that nafion does not react with hydrogen in the same way that negative electrode does. Thus, there should be no direct contribution of nafion to the discharge capacity.

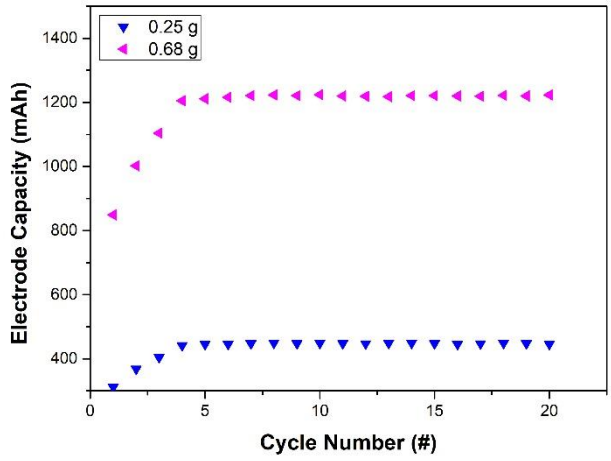

Figure 4.10 *Variation of the electrode capacity with increasing active material. The capacity normalized with respect to mass yields 448 mAh/g with 0.25 g and 451 mAh/g with 0.68 g of active material.*

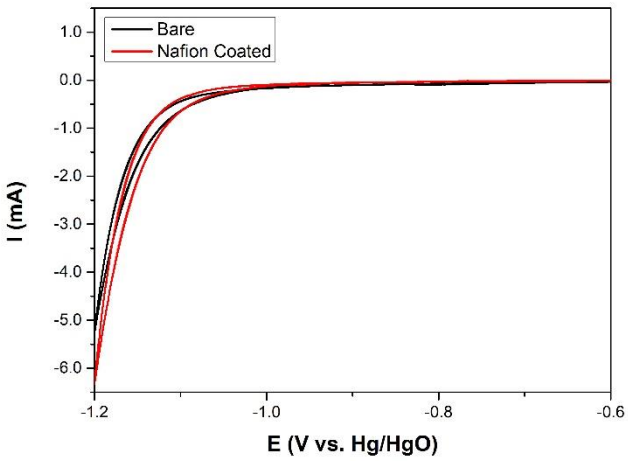

Figure 4.11 *CVs recorded from the bare and 2.80±0.09 µm nafion coated Ni mesh.*

CHAPTER 5

EFFECTS OF NAFION COATING ON ELECTROCHEMICAL PERFORMANCE OF METAL HYDRIDES

Studies reported in Chapter 3 and 4 indicates that nafion coating produces a number of alterations in the electrochemical performance of the electrode. These are which appear to be common both in $Mg_{50}Ni_{50}$ and A_2B_7 may be considered to have general applicability for all metal hydrides.

One important effect of nafion coating is that it increases the R_{ct} This was clearly shown in the present work where in the case of $Mg_{50}Ni_{50}$, the R_{ct} was increased from 4.62±0.16 Ω to 8.87±0.68 Ω and in the case of A_2B_7, the R_{ct} which had a value of 1.02±0.27 Ω with bare electrode was increased to 5.49±0.98 Ω. This is an expected result which would negatively affect the performance of the negative electrode.

The second important observation relates to voltammogram of nafion coated electrodes made from $Mg_{50}Ni_{50}$ and A_2B_7. The fact that both MH when coated with nafion display very similar voltammogram are very surprising. The voltammogram is a reflection of redox reactions taking place in active material of the electrode. These reactions in terms of discharge have different potentials in $Mg_{50}Ni_{50}$ (-0.81 V versus Hg/HgO) and A_2B_7 (-0.88 V versus Hg/HgO). How these potentials are brought to the same potentials by nafion coating is quite intriguing and require further investigation.

The third and most important observation in the current work was related to the increase in discharge capacity of the electrode with nafion coating. It should be re-emphasized that there is no direct contribution of nafion to the discharge capacity

of the electrode. The possibility of the surface effect which might cause this was also ruled out.

A possible explanation might be related to the indirect effect of modified thermodynamics that arises because of coating. During charging as the capacity is reached, hydrogen may tend to form bubbles. In the outer surface of nafion, which is expected to be quite flat, bubble formation is strained due to the difficulty of nucleation. In the inner surface of the nafion in contact with the electrode, bubble formation is much easier because of the roughness of the exposed metal hydride particles. But, such bubbles cannot escape from the surface due to nafion envelope which results in the increase of local hydrogen pressure, as schematically given in Fig. 5.1.

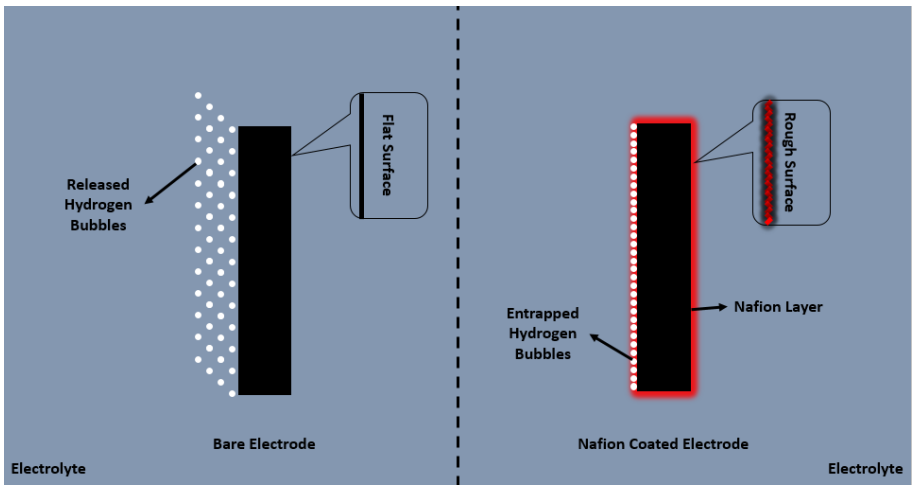

Figure 5.1 *Hydrogen bubble formation and disintegration at the electrode. Left side image represents the bare electrode and right side shows nafion coated electrode.*

For reasons given above, the local H_2 pressure on the electrode increases. As advanced by Tan et al. (2016), this results in a modified thermodynamics for the electrode. Fig. 5.2 shows a schematic PCT diagram of the active material. Here bare electrode makes use of storage capacity up to the bubbling pressure of hydrogen, normally 1 atm. With nafion coating, the local pressure increases well above that of bare electrode making the storage capacity higher.

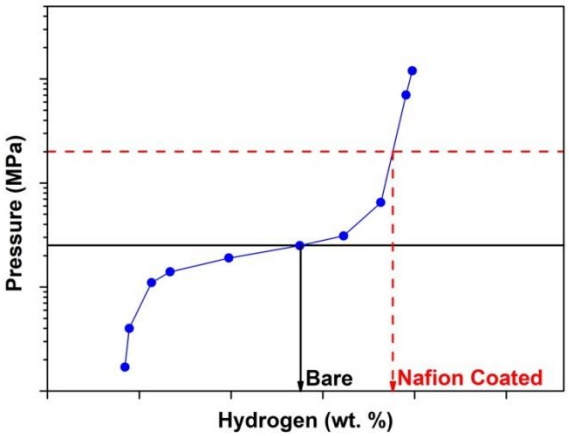

Figure 5.2 *Artificial PCT diagram of the electrode material showing the effect of pressure on the hydrogen storage capacity.*

CHAPTER 6

GENERAL CONCLUSIONS

The current study was undertaken to develop a negative electrode material for NiMH batteries with improved electrochemical performance and durability. The study was made up of two parts. In the first part, a Mg-based alloy, namely $Mg_{50}Ni_{50}$, which was synthesized via milling of elemental powders. The electrode prepared from this alloy was then coated with nafion to improve its durability. The following may be concluded from this study;

i. An amorphous $Mg_{50}Ni_{50}$ alloy comprising nanocrystalline Mg_2Ni phase was successfully synthesized from elemental powders with prolonged milling.
ii. The bare electrode prepared from $Mg_{50}Ni_{50}$ alloy yielded 329 mAh/g discharge capacity but exhibited a fast capacity decay. This capacity was reduced to 50 mAh/g after 20 cycles.
iii. Nafion coated electrode having a coating thickness of 2.80±0.09 μm yielded a higher discharge capacity, 498 mAh/g, in its first cycle. Nafion coating also improved capacity retention. After 20 cycles, the discharge capacity was still 387 mAh/g.

Findings reported above imply that nafion coating could be a beneficial to improve the durability of $Mg_{50}Ni_{50}$. Additionally, it also enhances the discharge capacity of electrodes.

In the second part, the origin of the increase in discharge capacity was investigated in alloys where the electrode was not significantly affected by an

alkaline environment. For this purpose, $(La_{0.70}Mg_{0.30})_2(Ni_{0.85}Co_{0.15})_7$ was selected as the alloy and the electrodes prepared from this alloy were tested electrochemically both in bare and nafion coated forms. This has shown that;

i. The bare alloy had a saturation capacity of 329 mAh/g, which was reached after 5 cycles. This capacity was increased up to 449 mAh/g with a nafion coating of 2.80±0.09 μm.
ii. The thickness of the nafion coating had a significant effect on the electrode capacity. It was found that the capacity scales with the nafion thickness; discharge capacities of 362 mAh/g, 383 mAh/g, and 449 mAh/g, were obtained with the nafion thicknesses of 0.70±0.05, 1.40±0.06 and 2.80±0.09 μm, respectively.

The increase in discharge capacity was attributed to the increased H_2 pressure on the electrode before they evolve as gas bubbles. This means that the alloy had an improved storage capacity may simply be provided by restrained bubbles in the nafion/electrode interface.

REFERENCES

Abe, T., Inoue, S., Mu, D., Hatano, Y., & Watanabe, K. (2003). Electrochemical studies of the effect of surface modification of amorphous MgNi electrodes by carbon or Ni. *Journal of Alloys and Compounds*, *349*(1–2), 279–283. https://doi.org/10.1016/S0925-8388(02)00901-5

Abe, T., Tachikawa, T., Hatano, Y., & Watanabe, K. (2002). Electrochemical behavior of amorphous MgNi as negative electrodes in rechargeable Ni-MH batteries. *Journal of Alloys and Compounds*, *330–332*, 792–795. https://doi.org/10.1016/S0925-8388(01)01589-4

Anik, M. (2009). Improvement of the electrochemical hydrogen storage performance of Mg2Ni by the partial replacements of Mg by Al, Ti and Zr. *Journal of Alloys and Compounds*, *486*(1–2), 109–114. https://doi.org/10.1016/j.jallcom.2009.06.127

Anik, M., Özdemir, G., Küükdeveci, N., & Baksan, B. (2011). Effect of Al, B, Ti and Zr additive elements on the electrochemical hydrogen storage performance of MgNi alloy. *International Journal of Hydrogen Energy*, *36*(2), 1568–1577. https://doi.org/10.1016/j.ijhydene.2010.10.087

Ayari, M., Ghodbane, O., & Abdellaoui, M. (2015). Elaboration and electrochemical characterization of LaTi2Cr4Ni5-based metal hydride alloys. *International Journal of Hydrogen Energy*, *40*(34). https://doi.org/10.1016/j.ijhydene.2015.06.169

Bala, H., Dymek, M., & Drulis, H. (2014). Development of metal hydride material efficient surface in conditions of galvanostatic charge/discharge cycling. *Materials Chemistry and Physics*, *148*(3), 1008–1012. https://doi.org/10.1016/j.matchemphys.2014.09.011

Brett, C. M. A., Alves, V. A., & Fungaro, D. A. (2001). Nafion-Coated Mercury Thin Film and Glassy Carbon Electrodes for Electroanalysis: Characterization by Electrochemical Impedance. *Electroanalysis*, *13*(3), 212–218. https://doi.org/10.1002/1521-4109(200103)13:3<212: AID-ELAN212>3.0.CO;2-Z

Chen, W., Zhu, Y., Yang, C., Zhang, J., Li, M., & Li, L. (2015). Significantly improved electrochemical hydrogen storage properties of magnesium nickel hydride modified with nano-nickel. *Journal of Power Sources*, *280*, 132–140. https://doi.org/10.1016/j.jpowsour.2015.01.089

Cui, N., Luan, B., Liu, H. K., & Dou, S. X. (1996). Discharge behavior of Mg2Ni-type hydrogen-storage alloy electrodes in 6 M KQH solution by electrochemical impedance spectroscopy The, *63*(96), 209–214.

Cui, N., Luan, B., Liu, H. K., Zhao, H. J., & Dou, S. X. (1995). Characteristics of magnesium-based hydrogen-storage alloy electrodes, *55*, 263–267.

Cui, N., & Luo, J. L. (1999). Electrochemical study of hydrogen diffusion behavior in Mg2Ni-type hydrogen storage alloy electrodes. *International Journal of Hydrogen Energy*, *24*, 26–31.

Durairajan, A., Haran, B. S., White, R. E., & Popov, B. N. (2000). Pulverization and corrosion studies of bare and cobalt-encapsulated metal hydride electrodes. *Journal of Power Sources*, *87*(1), 84–91. https://doi.org/10.1016/S0378-7753(99)00399-7

Etiemble, A., Rousselot, S., Guo, W., Idrissi, H., & Roué, L. (2013). Influence of Pd addition on the electrochemical performance of Mg-Ni-Ti-Al-based metal hydride for Ni-MH batteries. *International Journal of Hydrogen Energy*, *38*(17), 7169–7177. https://doi.org/10.1016/j.ijhydene.2013.03.080

Gamboa, S. a., Sebastian, P. J., Feng, F., Geng, M., & Northwood, D. O. (2002). Cyclic Voltammetry Investigation of a Metal Hydride Electrode for Nickel Metal

Hydride Batteries. *Journal of The Electrochemical Society*, *149*(2), A137. https://doi.org/10.1149/1.1430227

Gibb, J. R., & Thomas, R. P. (1948). Compounds of Hydrogen with Metals and Metalloids. *Journal of The Electrochemical Society*, *93*(5), 198. https://doi.org/10.1149/1.2773806

Goo, N. H., & Lee, K. S. (2002). The electrochemical hydriding properties of Mg – Ni – Zr amorphous alloy, *27*, 433–438.

Goo, N. H., Woo, J. H., & Lee, K. S. (1999). Mechanism of rapid degradation of nanostructured Mg2Ni hydrogen storage alloy electrode synthesized by mechanical alloying and the effect of mechanically coating with nickel. *Journal of Alloys and Compounds*, *288*(1–2), 286–293. https://doi.org/10.1016/S0925-8388(99)00100-0

Han, S. C., Jiang, J. J., Park, J. G., Jang, K. J., Chin, E. Y., & Lee, J. Y. (1999). Electrochemical evaluation of ball milled MgNi-based hydrogen storage alloys. *Journal of Alloys and Compounds*, *285*(1–2 Complete), 8–11. https://doi.org/10.1016/S0925-8388(99)00015-8

Hapçı Ağaoğlu, G., & Orhan, G. (2017). Elaboration and electrochemical characterization of Mg–Ni hydrogen storage alloy electrodes for Ni/MH batteries. *International Journal of Hydrogen Energy*, *42*(12), 8098–8108. https://doi.org/10.1016/j.ijhydene.2016.12.042

Hong, K. (2001). The development of hydrogen storage alloys and the progress of nickel hydride batteries. *Journal of Alloys and Compounds*, *321*(2), 307–313. https://doi.org/10.1016/S0925-8388(01)00957-4

Humana, R. M., Thomas, J. E., Ruiz, F., Real, S. G., Castro, E. B., & Visintin, A. (2012). Electrochemical behavior of metal hydride electrode with different particle size. *International Journal of Hydrogen Energy*, *37*(19), 14966–14971. https://doi.org/10.1016/j.ijhydene.2011.12.093

Jiang, J.-J., & Gasik, M. (2000). An electrochemical investigation of mechanical alloying of MgNi-based hydrogen storage alloys. *Journal of Power Sources*, *89*(1), 117–124. https://doi.org/10.1016/S0378-7753(00)00400-6

Kim, S. Y., Chourashiya, M. G., Park, C. N., & Park, C. J. (2013). Electrochemical performance of NAFION coated electrodes of hydriding combustion synthesized MgNi based composite hydride. *Materials Letters*, *93*, 81–84. https://doi.org/10.1016/j.matlet.2012.11.047

Kohno, T., Tsuruta, S., & Kanda, M. (1996). The hydrogen storage properties of new Mg2Ni alloy. *Journal of the Electrochemical Society*, *143*(9), L198–L199.

Kohno, T., Yamamoto, M., & Kanda, M. (1999). Electrochemical properties of mechanically ground Mg2Ni alloy. *Journal of Alloys and Compounds*, *293*, 643–647. https://doi.org/10.1016/S0925-8388(99)00358-8

Lee, H. Y., Goo, N. H., Jeong, W. T., & Lee, K. S. (2000). Surface state of nanocrystalline and amorphous Mg2Ni alloys prepared by mechanical alloying. *Journal of Alloys and Compounds*, *313*(1–2), 258–262. https://doi.org/10.1016/S0925-8388(00)01205-6

Lei, Y., Wu, Y., Yang, Q., Wu, J., & Wang, Q. (1994). Electrochemical Behavior of Some Mechanically Alloyed Mg-Ni-Based Amorphous Hydrogen Storage Alloys. *Zeitschrift Für Physikalische Chemie*, *183*, 379–384.

Li, X., Dong, H., Zhang, A., & Wei, Y. (2006). Electrochemical impedance and cyclic voltammetry characterization of a metal hydride electrode in alkaline electrolytes. *Journal of Alloys and Compounds*, *426*(1–2), 93–96. https://doi.org/10.1016/j.jallcom.2006.01.079

Linden, D. (2004). *Handbook of batteries*. *Cell*. https://doi.org/10.1016/0378-7753(86)80059-3

Liu, W., Lei, Y., Wu, J., & Wang, Q. (1997). The capacity deterioration model of mechanically alloyed MgXNi100-X amorphous electrodes in charging-

discharging cycling. *International Journal of Hydrogen Energy*, *22*(10–11), 999–1003. https://doi.org/10.1016/S0360-3199(96)00022-5

Liu, W., Wu, H., Lei, Y., & Wang, Q. (2002). Reaction kinetics of amorphous Mg50Ni50 hydride electrode. *Journal of Alloys and Compounds*, *346*(1–2), 244–249. https://doi.org/10.1016/S0925-8388(02)00488-7

Liu, W., Wu, H., Lei, Y., Wang, Q., & Wu, J. (1997). Effects of substitution of other elements for nickel in mechanically alloyed Mg50Ni50 amorphous alloys used for nickel—metal hydride batteries. *Journal of Alloys and Compounds*, *261*(1–2), 289–294. https://doi.org/10.1016/S0925-8388(97)00220-X

Liu, Y., Pan, H., Gao, M., & Wang, Q. (2011). Advanced hydrogen storage alloys for Ni/MH rechargeable batteries. *Journal of Materials Chemistry*, *21*(13), 4743. https://doi.org/10.1039/c0jm01921f

Lundqvist, A., & Lindbergh, G. (1999). Kinetic study of a porous metal hydride electrode. *Electrochimica Acta*, *44*(15), 2523–2542. https://doi.org/10.1016/S0013-4686(98)00380-6

Lutterotti, L. (2000). Maud: a Rietveld analysis program designed for the internet and experiment integration. *Acta Crystallographica*, *56*, s54. https://doi.org/10.1107/S0108767300021954

Ohara, R., Lan, C. H., & Hwang, C. S. (2013). Electrochemical and structural characterization of electroless nickel coating on Mg2Ni hydrogen storage alloy. *Journal of Alloys and Compounds*, *580*(SUPPL1). https://doi.org/10.1016/j.jallcom.2013.03.009

Orimo, S., & Fujii, H. (2001). Materials science of Mg-Ni-based new hydrides. *Applied Physics A*, *72*(2), 167–186. https://doi.org/10.1007/s003390100771

Ovshinsky, S. R., Fetcenko, M. A., & Ross, J. (1993). A Nickel Metal Hydride Battery for Electric Vehicles. *Science*, *260*(5105), 176–181. https://doi.org/10.1126/science.260.5105.176

Reilly, J., J., & Wiswall, R. H. (1968). Reaction of Hydrogen with Alloys of Magnesium and Nickel and the Formation of Mg2NiH4. *Inorganic Chemistry*, *7*(11), 2254–2256. Retrieved from http://pubs.acs.org/doi/pdf/10.1021/ic50069a016

Rongeat, C., Grosjean, M. H., Ruggeri, S., Dehmas, M., Bourlot, S., Marcotte, S., & Roué, L. (2006). Evaluation of different approaches for improving the cycle life of MgNi-based electrodes for Ni-MH batteries. *Journal of Power Sources*, *158*(1), 747–753. https://doi.org/10.1016/j.jpowsour.2005.09.006

Rongeat, C., & Roué, L. (2004). Effect of particle size on the electrode performance of MgNi hydrogen storage alloy. *Journal of Power Sources*, *132*(1–2), 302–308. https://doi.org/10.1016/j.jpowsour.2003.12.049

Ruggeri, S., Lenain, C., Roué, L., Liang, G., Huot, J., & Schulz, R. (2002). Mechanically driven crystallization of amorphous MgNi alloy during prolonged milling: Applications in Ni-MH batteries. *Journal of Alloys and Compounds*, *339*(1–2), 195–201. https://doi.org/10.1016/S0925-8388(01)01972-7

Sakai, T., Yuasa, A., Ishikawa, H., Miyamura, H., & Kuriyama, N. (1991). Nickel-metal hydride battery using microencapsulated alloys. *Journal of the Less Common Metals*, *172–174*, 1194–1204. https://doi.org/10.1016/S0022-5088(06)80027-5

Sandrock, G., & Thomas, G. (2001). The IEA/DOE/SNL on-line hydride databases. *Applied Physics A*, *72*(2), 153–155. https://doi.org/10.1007/s003390100770

Santos, S. F., de Castro, J. F. R., Ishikawa, T. T., & Ticianelli, E. A. (2007). Effect of transition metal additions on the electrochemical properties of a MgNi-based alloy. *Journal of Alloys and Compounds*, *434–435*(SPEC. ISS.), 756–759. https://doi.org/10.1016/j.jallcom.2006.08.153

Shahcheraghi, A., Dehghani, F., Raeissi, K., Saatchi, A., & Enayati, M. H. (2013). Effects of TiO2 additive on electrochemical hydrogen storage properties of nanocrystalline / amorphous Mg2Ni intermetallic alloy, *10*(1), 1–9.

Shao, H., Asano, K., Enoki, H., & Akiba, E. (2009). Preparation and hydrogen storage properties of nanostructured Mg-Ni BCC alloys. *Journal of Alloys and Compounds*, *477*(1–2), 301–306. https://doi.org/10.1016/j.jallcom.2008.11.004

Simičić, M. V., Zdujić, M., Dimitrijević, R., Nikolić-Bujanović, L., & Popović, N. H. (2006). Hydrogen absorption and electrochemical properties of Mg2Ni-type alloys synthesized by mechanical alloying. *Journal of Power Sources*, *158*(1), 730–734. https://doi.org/10.1016/j.jpowsour.2005.09.030

Souza, E. C., & Ticianelli, E. A. (2007). Structural and electrochemical properties of MgNi-based alloys with Ti, Pt and Pd additives. *International Journal of Hydrogen Energy*, *32*(18), 4917–4924. https://doi.org/10.1016/j.ijhydene.2007.07.024

Sun, D., Lei, Y., Liu, W., Jiang, J., Wu, J., & Wang, Q. (1995). The relation between the discharge capacity and cycling number of mechanically alloyed MgxNi100-x amorphous electrode alloys. *Journal of Alloys and Compounds*, *231*(1–2), 621–624. https://doi.org/10.1016/0925-8388(95)01739-9

Tan, S., Shen, Y., Onur Şahin, E., Noreus, D., & Öztürk, T. (2016). Activation behavior of an AB2 type metal hydride alloy for NiMH batteries. *International Journal of Hydrogen Energy*, *41*(23), 9948–9953. https://doi.org/10.1016/j.ijhydene.2016.03.196

Tarascon, J. M., & Armand, M. (2001). Issues and challenges facing rechargeable lithium batteries: Materials for clean energy. *Nature*, *414*, 359–367.

Uluc, A. V., Mol, J. M. C., Terryn, H., & Böttger, A. J. (2014). Hydrogen sorption and desorption related properties of Pd-alloys determined by cyclic voltammetry.

Journal of Electroanalytical Chemistry, *734*, 53–60. https://doi.org/10.1016/j.jelechem.2014.09.021

Wang, C., Wang, S., Peng, L., Zhang, J., Shao, Z., Huang, J., … He, X. (2016). Recent progress on the key materials and components for proton exchange membrane fuel cells in vehicle applications. *Energies*, *9*(8). https://doi.org/10.3390/en9080603

Wang, H., Han, L., Hu, H., & Northwood, D. O. (2009). The hydrolysis behavior of Mg2Ni and Mg2NiH4 in water or a 6 M KOH solution and its application to Ni nanoparticles synthesis. *Journal of Alloys and Compounds*, *470*(1–2), 539–543. https://doi.org/10.1016/j.jallcom.2008.03.016

Woo, J. H., & Lee, K. S. (1999). Electrode Characteristics of Nanostructured Mg 2 Ni-Type Alloys Prepared by Mechanical Alloying, *146*(3), 819–823.

Yang, C., Zhu, Y., Zhang, W., Zhu, J., & Li, L. (2011). Effects of metal doping on electrochemical properties of Mg-based hydrogen storage alloys. *Journal of Nanjing University of Technology*, *33*(4), 52–57.

Yiwen, C., Yungui, C., Ding, Z., Chaoling, W., & Dongliang, C. (2013). Electrochemical Performance Improvement of AB5-type Metal Hydride Electrode by Adding KF in KOH Electrolyte. *Rare Metal Materials and Engineering*. https://doi.org/10.1016/S1875-5372(13)60065-X

Zhang, B., Wu, W., Bian, X., & Tu, G. (2013). Investigations on rate constants of the charging/discharging processes for metal hydride electrodes. *Electrochimica Acta*, *87*, 645–650. https://doi.org/10.1016/j.electacta.2012.10.004

Zhang, Y. H., Li, B. W., Ren, H. P., Hu, F., Zhang, G. F., & Guo, S. H. (2011). Gaseous and electrochemical hydrogen storage kinetics of nanocrystalline Mg2Ni-type alloy prepared by rapid quenching. *Journal of Alloys and Compounds*, *509*(18), 5604–5610. https://doi.org/10.1016/j.jallcom.2011.02.085

Zhang, Y. H., Lü, K., Zhao, D. L., Guo, S. H., Qi, Y., & Wang, X. L. (2011). Electrochemical hydrogen storage characteristics of nanocrystalline and amorphous Mg2Ni-type alloys prepared by melt-spinning. *Transactions of Nonferrous Metals Society of China (English Edition)*, *21*(3), 502–511. https://doi.org/10.1016/S1003-6326(11)60743-7

Zhang, Y., Han, X., Li, B., Ren, H., Dong, X., & Wang, X. (2008). Electrochemical characteristics of Mg2−xZrxNi (x=0–0.6) electrode alloys prepared by mechanical alloying. *Journal of Alloys and Compounds*, *450*(1–2), 208–214. https://doi.org/10.1016/j.jallcom.2006.10.079

Zhang, Y., Zhao, D., Han, X., Li, B., Dong, X., & Wang, X. (2007). Electrochemical characteristics of mechanical alloyed (Mg1−xZrx)2Ni (x=0.0.1) electrode alloys. *International Journal of Hydrogen Energy*, *32*, 2830. https://doi.org/10.1016/j.ijhydene.2007.01.008

Zhang, Z., Elkedim, O., Balcerzak, M., & Jurczyk, M. (2016). Structural and electrochemical hydrogen storage properties of MgTiNiX (x = 0.1, 0.5, 1, 2) alloys prepared by ball milling. *International Journal of Hydrogen Energy*, *41*(27). https://doi.org/10.1016/j.ijhydene.2015.11.168

APPENDIX

CARBON ENCAPSULATION OF MAGNESIUM PARTICLES

A.1 Introduction

Magnesium is an attractive metal for a number of applications. One of these is hydrogen which can be stored in large quantities. Such hydrogen storage alloys can be used as negative electrode material in metal hydride batteries. Currently common alloy in use for this purpose is Mischmetal (rare-earth alloy) based AB_5 type of an alloy (A: Mm, La, Ce, Ti; B: Ni, Co, Mn, Al). Magnesium is even better than this alloy since the amount of hydrogen that it can store is nearly 5 times that of the current alloy. However, there are a number of problems to be solved if Mg is to be used as negative electrode material. These are that MgH_2 is too stable for such purposes and it needs to be destabilized, kinetics of hydrogenation and dehydrogenation needs to be accelerated

There is one additional problem which is common to Mg and Mg based alloys. Environment in metal hydride batteries is alkaline and Mg is subject to corrosion in this environment. Thus, if Mg and Mg based alloys are to be used as negative electrode material, they need to be protected from this environment. This study concentrates on this problem and examines the possibility of protecting Mg with carbon encapsulation. Mg powders coated with carbon via a solvothermal method. Two agents were used in the encapsulation were sucrose and citric acid.

A.2 Materials and Methods

The method with sucrose is as follows. The sucrose was dissolved in in a suitable solution (ethanol, methanol, acetone, deionized water). The solution was mixed with Mg powders, being -325 mesh in size (Alfa Aesar, 99.8%), keeping

Mg:C=95:5. After the partial vaporization of the solution, a gel-like mixture was obtained. This gel placed into a tube furnace and heated to the 300°C with a rate of 5°C/min. for pyrolysis. This was carried out under nitrogen flow (8 slph) so as to prevent oxidation and remove the by-products of the pyrolysis from the furnace atmosphere.

In the second set of experiments, the exactly same procedure was followed by replacing sucrose with citric acid.

The resulting encapsulated powders were characterized with SEM (JEOL JSM6400) so as to observe the morphology of encapsulation. Encapsulated powders were also examined with Raman spectroscopy (Bruker IFS 66/S) as well as with X-ray diffraction (Rigaku DMAX 2200).

The extent to which encapsulated powders were resistant to corrosion was examined with a set-up given in Fig. A.1. Here the set-up consists of an Erlenmeyer flask of 250 ml connected to a volumetric gas collecting cylinder. A typically 2.5 g of encapsulated powder was placed at the bottom of the flask.

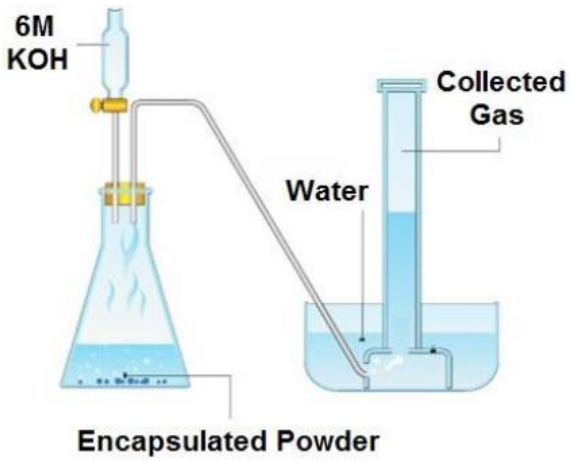

Figure A.1 *Schematic view of the corrosion test setup. Gaseous product of the corrosion reaction is collected at the volumetric flask taking place at the left side.*

The experiment was started by pouring 100 ml 6M KOH into it. This is expected to produce hydrogen gas, according to the reaction provided below as:

$$Mg + H_2O \rightarrow Mg(OH)_2 + H_2$$ ***Equation A.1***

Encapsulated powders were also characterized with regard to their resistivity. For this purpose, encapsulated powders were poured into a die and pressed into a pellet, 18 mm diameter and 0.5 mm in thickness by single action pressing.

Resistivity values were calculated from the resistance measured with a homemade four-point-probe tester. The measuring probes were coated with gold to minimize errors due to the internal resistance of the probe needles. The distance between the testing probes were 4 mm. since in case of higher sample thicknesses than the 40% of the inter-probe distance, resistance cannot be measured correctly. Measurements were carried out at room temperature and the resistance, R, obtained from samples were converted into resistivity, ρ, using the relation;

$$\rho = 2\pi sFR$$ ***Equation A.2***

where s is the inter-probe distance (m) and F is the correction factor (0.81) for the sample geometry.

A.3 Results and Discussions

Initial experiments were carried with sucrose-acetone. Three different temperatures were employed; 400, 350 and 300°C, heating rate being the same in all experiments. It was noticed that Mg vaporizes at 400°C and to be on the safe side, 300°C was selected as pyrolysis temperature. Next, a number of experiments were carried with different pyrolysis time; 4, 6, 8, 10 hours. After 8 hours of pyrolysis, the mixture was fully hardened and powders could not be regained. Therefore, pyrolysis was carried out for 6 hours.

A typical SEM image of Mg and encapsulated Mg powders are given in Fig.A.2. Here Mg encapsulated with sucrose-acetone appears quite satisfactory, Fig. A.2 (b) in terms of appearance, but it charges heavily under SEM implying that it is not conductive enough. In addition to the charging problem, organic traces due to the incomplete pyrolysis were also detected in the SEM images of the sucrose-acetone used encapsulation route.

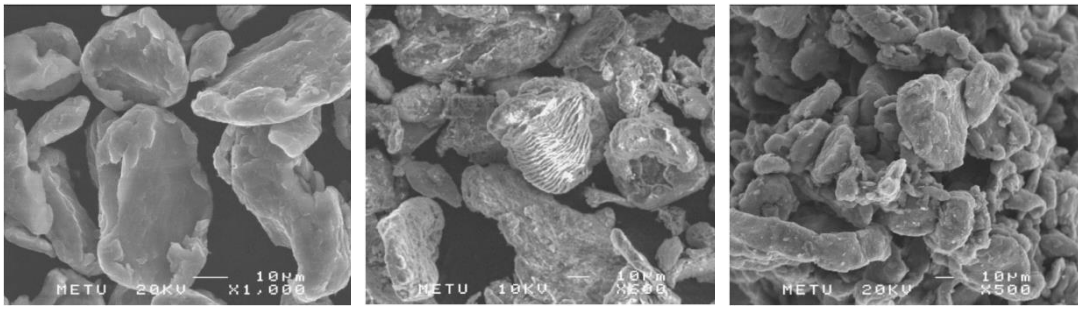

(a) (b) (c)

Figure A.2 *SEM images for a) Starting Mg powder b) Mg encapsulated with sucrose-acetone c) Mg encapsulated with citric acid-acetone.*

In order to obtain more satisfactory coating, following the studies, sucrose was replaced with citric acid. Since the solubility of citric acid in acetone is rather small, alternative solvents, namely methanol, ethanol and deionized water were used. Unfortunately, all of these solvents led to oxidation of Mg (see Fig. A.3). Therefore, the original solvent, acetone, was continued to be used and limited solubility was overcome by the use of excess solvent.

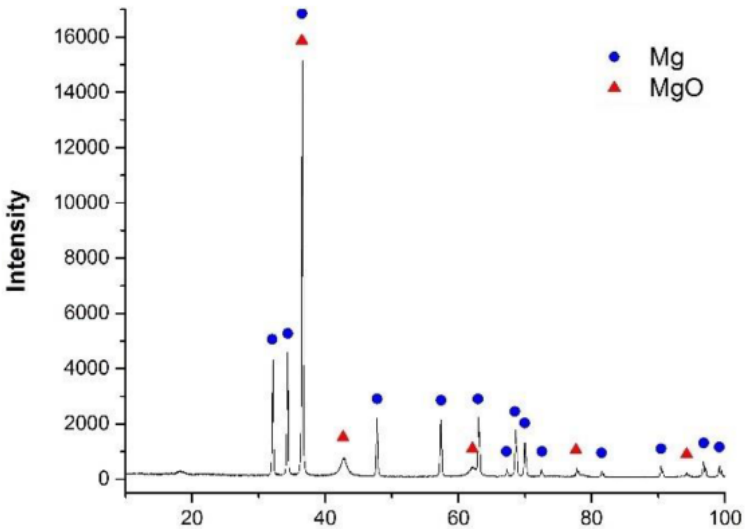

Figure A.3 *XRD spectrum of the encapsulated powders by using citric acid and ethanol. Rietveld analysis conducted on the powders revealed that the amount of MgO formed is 19.1 at. % (Bragg R-factor: 7.8, reduced $\chi 2$: 7.8).*

An example of Mg powders encapsulated with citric acid-acetone is given in Fig. A.2 (c). The sample charges very little indicating that it has better conductivity as compared to previous samples. Also, powders have the same appearances as the initial powder compare Fig. A.2 (c) with Fig A.2 (a).

Results of corrosion experiments are given in Table 1. The table comprises values referred to gas collected from powders coated with sucrose-acetone and citric acid- acetone routes. Pure Mg was also included for comparison. As seen in the table Mg encapsulated with sucrose-acetone route produces 24 ml. H_2 gas within 24 hours. Pure Mg produces H_2 which larger than the capacity of the measuring cylinder (> 80 ml.). The best result was obtained with Mg powder encapsulated with citric acid- acetone route. The value was one fourth of that collected with sucrose-acetone route, i.e. 6 ml. gas collected after the 24 hours of exposure to the 6M KOH solution.

Table A.1 *Corrosion test results showing the amounts of collected gas after 24 hours.*

Material	Collected Gas (ml)
Mg	>80
Mg-Sucrose @Acetone	≈24
Mg-Citric Acid @Acetone	≈6

Resistivity values obtained for the samples at room temperature are given in Table A.2. It should be noted that the resistivity values in sucrose route is 3 orders of magnitude larger than those obtained with citric acid route. Thus, resistivity measurements also imply that the coating has a better conductivity with citric acid.

Table A.2 *Resistivity data of the samples obtained with 4-probe resistivity measurement.*

Material	Electrical Resistivity (nΩ×m)
Mg	105.9±2.8
Mg-Sucrose @Acetone	$27.8\times10^{3}\pm30.6$
Mg-Citric Acid @Acetone	759.1±5.2

Mg encapsulated via citric acid route was also examined with Raman spectroscopy. The spectrum recorded is given in Fig. A.4. The spectrum, despite pyrolysis still shows the bonds other than C-C, e.g. C-H which implies that the pyrolysis is not yet complete. Peaks labeled at carbon represents the D band (1336 cm^{-1}), G band (1568 cm^{-1}) and 2D band (2660 cm^{-1}), respectively, which should be clearly resolved in an appropriately pyrolyzed sample having a carbon-based encapsulation layer.

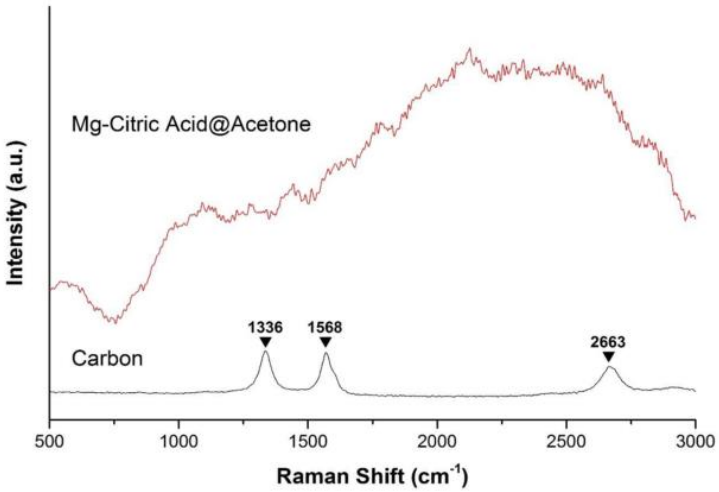

Figure A.4 *Raman spectrum of the encapsulated Mg with citric acid-acetone in comparison with the carbon.*

A.4 Conclusions

In the current work, Mg powders were encapsulated with a solvothermal method for the purpose of preventing the corrosion in alkaline environments. The study has shown the followings:

i. Mg powder can be encapsulated with sucrose or citric acid using acetone as a solvent.
ii. The use of other solvents such as ethanol methanol or deionized water is not recommended as a solvent because they tend to oxide Mg powder

iii. Of the two routes, citric acid is a better encapsulating agent as it provides a better protection of Mg as verified by gas collecting experiments and resistivity measurements

Lastly it should be mentioned that even with citric acid, Mg could not be fully protected as there is still H_2 gas evolution as it contacts with KOH solution. This is consistent with Raman measurement which implies that the pyrolysis is not complete at 300°C. The use of higher pyrolysis temperature, e.g. 350°C, maybe recommended for a better encapsulation.

A.5 References

Ngo, D. T., Kalubarme, R. S., Chourashiya, M., Park, C., & Park, C. (2014). Electrochemical Performance of GeO2/C Core Shell based Electrodes for Li-ion Batteries. *Electrochimica Acta*, *116*, 203-209. doi:10.1016/j.electacta.2013.11.031

Wang, H., Zhang, J., Liu, J. W., Ouyang, L. Z., & Zhu, M. (2013). Improving hydrogen storage properties of MgH2 by addition of alkali hydroxides. *International Journal of Hydrogen Energy*, *38*(25), 10932-10938. doi:10.1016/j.ijhydene.2013.02.075

Ying, T. K., Gao, X. P., Hu, W. K., Wu, F., & Noreus, D. (2006). Studies on rechargeable NiMH batteries. *International Journal of Hydrogen Energy*, *31*(4), 525-530. doi:10.1016/j.ijhydene.2005.04.018

Zhang, S., Deng, C., Liu, F. L., Wu, Q., Zhang, M., Meng, F. L., & Gao, H. (2013). Impacts of in situ carbon coating on the structural, morphological and electrochemical characteristics of Li2MnSiO4 prepared by a citric acid assisted sol–gel method. *Journal of Electroanalytical Chemistry*, *689*, 88-95. doi:10.1016/j.jelechem.2012.11.028

Zhao, X., & Ma, L. (2009). Recent progress in hydrogen storage alloys for nickel/metal hydride secondary batteries. *International Journal of Hydrogen Energy*, *34*(11), 4788-4796. doi:10.1016/j.ijhydene.2009.03.023